

BATTERY-FREE WIRELESS PRESSURE SENSOR

By

JOSE GREGORIO VILLALOBOS JIMENEZ

A thesis submitted in partial fulfillment of the requirements for the degree of

MASTER OF SCIENCE

in

MECHANICAL ENGINEERING

UNIVERSITY OF PUERTO RICO

MAYAGÜEZ CAMPUS

2010

Approved by:

David Serrano, ScD
Member, Graduate Committee

Date

Fredrick A. Just Agosto,, Ph.D
Member, Graduate Committee

Date

Yi Jia, Ph.D
President, Graduate Committee

Date

Mario Padron Corbera, Ph.d
Representative of Graduate Studies

Date

Gustavo Gutierrez, Ph.D
Chairperson of the Department

Date

Abstract of Dissertation Presented to the Graduate School
of the University of Puerto Rico in Partial Fulfillment of the
Requirements for the Degree of Master of Science

BATTERY-FREE WIRELESS PRESSURE SENSOR

By

JOSE GREGORIO VILLALOBOS JIMENEZ

December 2009

Chair: YI JIA

Major Department: Department of Mechanical Engineering

In this project two different battery-free wireless pressure sensors have been developed with the same structure with two major parts: a capacitor that serves as a pressure sensing element and an inductor which works as a passive power source and data communication element. These two components work together as an LC resonator to realize the wireless pressure sensing and remote power to eliminate the need for wire connection. The first pressure sensor has a laminated structure with an interdigital capacitor (IDC) that is a sensing element and an inductor coil as antenna, the sensing element is comprised of a set of linear parallel electrodes coated with Polyvinylidene Fluoride (PVDF) pressure sensing material on the top. The change of capacitance in the IDC is a function of the geometry of the electrodes and the electric properties the sensitive layer. The sensing element for the second pressure sensor is a parallel plate which the change the capacitance is due the deformation of the dielectric material between the conductive parallel plates; for this pressure sensor design two kind of polymeric materials (liquid rubber of polyurethane and Polydimethylsiloxane) have been used and it; these materials must be soft enough to deform over a target pressure. The inductor coil was formed by winding an insulated

wire. The inductor coil was formed by winding an insulated wire . The interdigital prototype shows an experimental response to measure a range of pressure from 0 psi to 60 psi with an average sensitivity of 25KHz/psi and the parallel plates were designed to measure a range of pressure from 0 psi to 48 psi with an average sensitivity of 33.3 KHz/psi and 66.6 KHz/psi for PDMS and Polyurethane, respectively.

Resumen de Disertación Presentado a Escuela Graduada
de la Universidad de Puerto Rico como requisito parcial de los
Requerimientos para el grado de Maestría en Ciencias

TITULO DE LA TESIS

Por

JOSE GREGORIO VILLALOBOS JIMENEZ

Julio 2009

Consejero: YI JIA

Departamento: Departamento de Ingenieria Mecanica

En este proyecto seran propuestos dos diferentes sensores pasivos inalambricos de presion los cuales tienen la misma estructura con dos partes principales: un capacitor que sirve como elemento sensante de presin y un inductor que trabaja como fuente pasiva de poder y elemento de transmision de datos. Estos dos componentes trabajan juntos como un circuito resonador LC para realizar la medicion inalambrica de la presion, eliminando la necesidad de de conexion por cables. EL primer sensor tiene una estructura laminada con un capacitor interdigital (IDC) que es el elemento sensante y un inductor en forma de bobina, el elemento sensante esta compuesto por un juego electrodos lineales y paralelos cubiertos con Polyvinylidene Fluoride (PVDF) en la parte superior. El cambio de capacitancia en el capacitor interdigital es una funcin de la geometra de los electrodos y las propiedades elctricas del material sensitivo encima de los electrodos. El elemento sensante para el segundo sensor propuesto son unas placas paralelas las cuales el cambio de capacitancia es debido a la deformacion de material dielectrico entre las placas paralelas conductoras. Para este diseo de este sensor de presin dos clases de materiales polimricos (Poliuretano y Polydimethylsiloxane) han sido utilizados ; estos materiales deben ser

lo suficientemente suaves para que se puedan deformar bajo una presión específica. El inductor está formado por una bobina con un cable aislado. El prototipo interdigital muestra una respuesta experimental para medir un rango de presión de 0 psi a 60 psi con una sensibilidad promedio de 25 KHz/psi y los prototipos de placas paralelas fueron mostraron una respuesta experimental para medir un rango de presión entre 0 psi a 48 psi con una sensibilidad promedio de 33.3 KHz/psi y 66.6 KHz/psi para el Polydimethylsiloxane y poliuretano respectivamente.

Copyright © 2009

by

JOSE GREGORIO VILLALOBOS JIMENEZ

To my parents

ACKNOWLEDGMENTS

I wish to express my gratitude to my thesis advisor, Professor Yi Jia, who gave me the opportunity to join his group in the January of 2008. I feel grateful for having been offered a chance to study passive wireless sensing technology in his research group. I am also grateful for his continuous support and encouragement that he offered me in the progress of the project.

I would like to thank my family for their unconditional support, inspiration and love.

Funding and resources for the development of this research were provided by NSF Grant 0549338 and DE-FG26-07NT43061.

TABLE OF CONTENTS

	<u>page</u>
ABSTRACT ENGLISH	ii
ABSTRACT SPANISH	iv
ACKNOWLEDGMENTS	viii
LIST OF TABLES	xi
LIST OF FIGURES	xii
LIST OF SYMBOLS	xiv
1 INTRODUCTION	1
1.1 Background	1
1.2 Proposed Passive Wireless Pressure Sensors	3
1.2.1 Principle Of Operation	3
1.2.2 Parallel Plate Pressure Sensor	4
1.2.3 Interdigital Pressure Sensor	5
1.3 Advantages Of Passive Wireless Sensing Technology	6
1.4 Research Objectives	7
1.5 Thesis Organization	8
2 LITERATURE REVIEW	9
2.1 Traditional Pressure Sensing Devices	9
2.2 Strain Gauge Pressure Sensors	10
2.3 Potentiometric Pressure Sensors	11
2.4 Resonant-Wire Pressure Sensors	11
2.5 Inductive Pressure Sensors.	12
2.6 Piezoresistive Pressure Sensors	12
2.7 Strain Gauge Transducers	13
2.8 Capacitive Pressure Sensors	13
2.9 Wireless Sensing Technology	15
2.9.1 Commercial Wireless Sensor Platforms	15
2.9.2 Radio Frequency Identification Based Sensors	16
2.9.3 Wireless SAW Sensors	17
2.9.4 RF Powered LC Sensors	18
2.10 Conclusions	21

3	BATTERY-FREE WIRELESS PRESSURE SENSOR DESIGN	22
3.1	Parallel Plate Capacitor	22
3.1.1	Parallel Plate Sensor Design	24
3.2	Interdigital Capacitor	28
3.2.1	Interdigital Capacitance Analysis	31
3.2.2	Geometry Dependent IDC Capacitance	38
3.2.3	Simulation of the electrostatic field of IDC	40
3.2.4	Pressure Dependent Capacitance	45
3.3	Spiral Inductor	46
3.3.1	Self- Inductance	46
3.3.2	Mutual Inductance	47
4	PERFORMANCE ANALYSIS	49
4.1	Modeling and Simulation	49
4.2	Performance Analysis	55
4.2.1	Resonant Frequency	55
4.2.2	Q-factor	57
4.2.3	Coupling Factor	58
4.3	Conclusions	59
5	SENSOR FABRICATION AND EXPERIMENTAL RESULTS	61
5.1	Fabrication Parallel Plates Pressure Sensor	61
5.2	Fabrication Interdigital Pressure Sensor	64
5.3	Experimental Results	67
5.3.1	Parallel Plate	69
5.3.2	Interdigital Pressure Sensor	71
5.4	Conclusions	72
6	CONCLUSION AND FUTURE WORK	73
6.1	Conclusion	73
6.2	Future Work	74
	APPENDICES	75
A	TITLE OF APPENDIX A	76

LIST OF TABLES

<u>Table</u>		<u>page</u>
3-1	Electrical Parameter Values	28
3-2	Detailed equations needed for the calculation of CI and CE for a finite layer as well as for an infinite layers	36
3-3	Electrical Parameter Values	39
4-1	Electrical Parameter Values	52
4-2	Electrical Parameter Values for Interdigital sensor	52

LIST OF FIGURES

Figure	page
1-1 Schematic of a battery-free passive wireless sensing system	4
1-2 Schematic parallel plates pressure sensing element	5
1-3 Schematic Interdigital Pressure sensor	6
1-4 Proposed Wireless Pressure Sensing System	7
2-1 Typical pressure sensor’s functional blocks	10
2-2 Car tire incorporating RFID pressure sensor readable from the car . .	18
2-3 The working principle of the LC pressure and temperature sensor . .	20
3-1 A parallel-plate capacitor	22
3-2 The electric field between the plates of a parallel-plate capacitor . . .	23
3-3 Schematic view of the parallel pressure sensor when is applied a pressure	25
3-4 Parallel plate pressure sensor design	27
3-5 Operating principle of interdigital sensor	29
3-6 A schematic view of the interdigital capacitor simplification.	30
3-7 2-dimensional cross-sectional view of the IDC with the geometric di- mensions	32
3-8 Schematic view of the IDC on the test machine	32
3-9 A half unit cell model of the proposed multilayer IDC	34
3-10 The equivalent circuit of the static capacitance of a multilayer inter- digital capacitor	34
3-11 Splitting of the proposed three-layered IDC	35
3-12 Capacitance as a funtion of η , for a IDC designed with the parameter of the table 3-3	40
3-13 Design of the IDC in Comsol	42

3-14 Mesh of the simulation	43
3-15 Result for the capacitance for the IDC simulation	43
3-16 Simulation plots results for the electric potential [V]	44
3-17 Changing current in coil 1 produces changing magnetic flux in coil 2	47
4-1 Inductive Coupled Reader and LC Sensor	49
4-2 Equivalent Circuit Diagram of Wireless Telemetry System	50
4-3 Magnitude and Phase Angle of Zs Polyurethane	53
4-4 Magnitude and Phase Angle of Zs PDMS Parallel Plate	54
4-5 Resonant Frequency of Input Impedance vs. Pressure IDC PVDF	55
5-1 Detailed Fabrication Process for parallel plate pressure sensor	62
5-2 Sensor Prototype of parallel plate pressure sensor	63
5-3 Lateral view of Prototype for PDMS material	63
5-4 Sensor Prototype of IDC pressure sensor	65
5-5 Illustration on the sensor fabrication using photolithography.	66
5-6 Schematic view of the compression testing machine	67
5-7 Principle of Sensor Calibration Experiment	68
5-8 Calibration test setup up	68
5-9 Resonant frequency of the tank vs. pressure measured with the wire- less set-up for POLYURETHANE material	69
5-10 Resonant frequency of the tank vs. pressure measured with the wire- less set-up for PDMS material	70
5-11 Resonant frequency of the tank vs. impedance response of the reader measured with the wireless set-up for PDMS material	70
5-12 Resonant frequency of the tank vs. pressure measured with the wire- less set-up for POLYURETHANE material	71
5-13 Resonant frequency vs. pressure measured for the IDC sensor	72

LIST OF SYMBOLS

SYMBOL	NAME	UNIT
A	Sensing area of the sensor	mm^2
a	Coil wire radius	mm
C_R	Capacitance of the reader	F
C_S	Capacitance of the sensor	F
f	Resonant frequency	Hz
I_1	Current on the reader antenna	A
I_2	Current on the sensor	A
k	Coupling Coefficient	/
L_R	Inductance of the reader	H
L_S	Inductance of the sensor	H
M	Mutual inductance	H
n	Turns of the coil	/
R	Coil loop radius	mm
R_R	Self resistance of the reader	Ω
R_S	Self resistance of the sensor	Ω
t	Thickness of the sensing material	mm
ϵ_0	Permittivity of free space 8.85×10^{-12}	F/m
μ_0	Magnetic permeability of free space $4\pi \times 10^{-7}$	H/m
η	Metallization Ratio Interdigital Capacitor	/
λ	Spatial Wavelength Interdigital Capacitor	/

1 INTRODUCTION

This chapter starts with the background introduction of this thesis project, followed by the description of proposed battery-free passive wireless Pressure Sensor for Structural Health Monitoring, and finally an overview and organization of the thesis is presented.

1.1 Background

In the recent years there has been an increasing interest in the use of sensing technologies for Structural Health Monitoring (SHM) systems. Wireless sensor and sensor networks have begun to consider as substitutes for traditional tethered monitoring systems [1]. Structural monitoring systems can be found in systems such as aircrafts, ships, and civil structures and these systems are responsible for collecting the measurement from the sensors and store the data within a central data acquisition. To assure reliability of the data, the structural monitoring systems use wires for communication between the sensors and the central data acquisition. While the wires provide a good communication, the installation can be expensive and labor-intensive. The high cost of installation is not only for tall buildings and civil structures but also within aircrafts, ships and other structural systems [2, 3]. Researchers have developed different wireless active sensors for localized SHM [4, 5] these kind of sensor meet the requirements for SHM but batteries are the common power source for most of active wireless sensors and when batteries are exhausted and is it difficult to change a battery periodically. Nowadays there is an increasing need for industrial pressure sensors and the range of operation for pressure and temperature

of these devices is high and most of these devices are used for plant regulation and control to ambient monitoring; examples of industry applications for pressure sensor include automotive industry, medical, consumer, aviation, defense, pneumatic and hydraulic systems, space exploration and oil drilling industry [6–9] for many of these applications is needed sensors that are wireless and do not require power supplies. In addition to typical industry applications, pressure sensors within living organisms have been studied and developed [10–12]. Most of the industrial applications have harsh environments for pressure sensor for instance in combustion engine where a robust pressure sensor using high-temperature material has to be developed in order to enhance fuel efficiency, reduce emissions and improve reliability of the vehicles [13]. The cost of the devices sensing must be low enough in industrial applications to allow such technology insertion.

In this project is proposed two pressure sensors which have the same structure with two major parts: a capacitor which is a pressure sensing element and an inductor that works as a passive power source and data communication element. These two components work together as an LC resonator to realize the wireless pressure sensing and remote power, eliminating the need for wire connection. The first proposed pressure sensor has a laminated structure with an interdigital capacitor (IDC) that is a sensing element and a inductor coil that works as a passive power source and data communication element, for this proposed sensor the sensing element is comprised of a set of linear parallel electrodes coated with Polyvinylidene Fluoride (PVDF) as pressure sensing material on the top. The change of capacitance in the IDC is a function of the geometry of the electrodes and the electric properties the sensitive layer (PVDF film). The sensing element for the second proposed pressure sensor is a parallel plate which the change of the capacitance is due the deformation of the dielectric material between the conductive parallel plates. For this design a

polymeric liquid material will be used and it has to be soft enough to deform over a target pressure. The inductor coil will be formed by winding an insulated wire.

1.2 Proposed Passive Wireless Pressure Sensors

This work presents a battery-Free wireless pressure sensor which has a LC resonant circuit and is activated by electromagnetic waves and the resonant frequency of the sensor is interrogated remotely with a single loop antenna by applying an oscillating signal to the antenna and monitoring the frequency response voltage across it.

1.2.1 Principle Of Operation

Principle of the proposed pressure wireless sensing is based on the operation of an inductor-capacitor (L-C) tuned electric oscillator. The oscillator LC consists of an inductor and a capacitor in parallel. Its operation is based on the storage of energy in the form of electric charge in the capacitor and in the form of magnetic field in the inductor. The property which we want to sense, such as pressure, induced the variation of sensor capacitance due to sensing parameter variation. The remote reader detected this information by monitoring resonant frequency variations due to impedance changes in response to property sensed. The characteristic of this type of L-C circuit tank, is that the velocity which the current flows from the capacitor to the inductor or vice versa, is produced with a frequency (F), called frequency of resonance, that depends on the values of the capacitor (C) and the inductor (L), and is expressed by the equation 1.1

$$F = \frac{1}{2\pi\sqrt{LC}} \quad (1.1)$$

The Figure 1.1 shows the schematic of a battery-free passive wireless sensing system. It consists of a sensor unit, which does not have any power source of its own, and

a transceiver unit, which provides energy to the sensor. The sensor provides information back to the transceiver via the inductive link. A polyimide film protection layer is used to isolate the entire sensor from possible chemical erosion and electrical shorts. The planar spiral inductor collects electromagnetic energy from the environment and delivers the strain information back to the reader. As a sensing element, the interdigital capacitor is comprised of a set of linear parallel electrodes. The electrodes consist of two series of electrodes with opposite polarities.

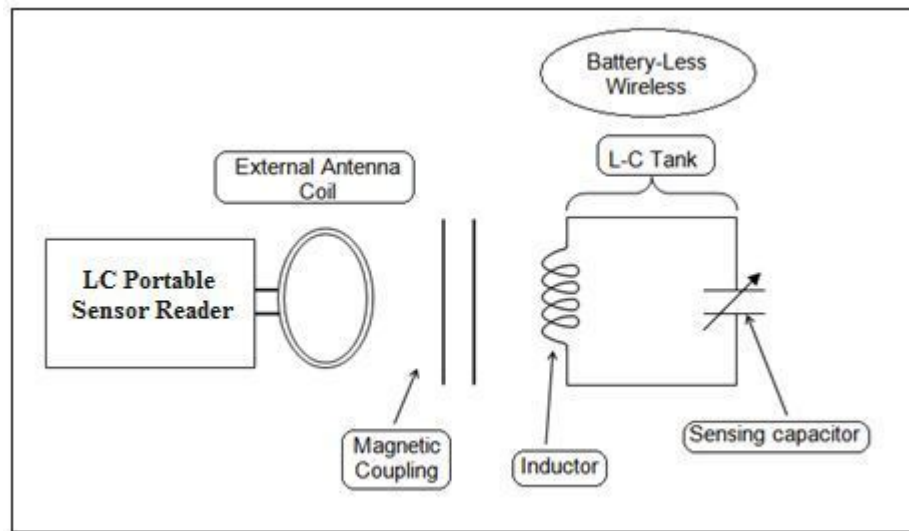


Figure 1-1: Schematic of a battery-free passive wireless sensing system

1.2.2 Parallel Plate Pressure Sensor

For the proposed parallel plate pressure sensor, the change of capacitance is due to the deformation of the dielectric material between the conductive parallel plates. The device is constructed with two metal plates and an intermediate material layer that is soft enough to deform in a pressure range. Most of capacitive pressure sensors use an elastic diaphragm with fixed edges and sealed cavity in between the diaphragm and the substrate below this configuration can produce leaks. The goal of this research for the proposed parallel plate sensor is to eliminate the need of diaphragms and cavities from the common micromachined capacitive sensors and fabricate a capacitive pressure sensor that can be used in environments with high

pressure or mechanical robustness using metal plates with an intermediate polymer layer. Some micromachined sensors have been designed using sandwich-type constructions with deformable intermediate layers[14, 15] as well as commercial pressure mapping systems [16]. In the figure 1-2 is shown an schematic view of the parallel plates.

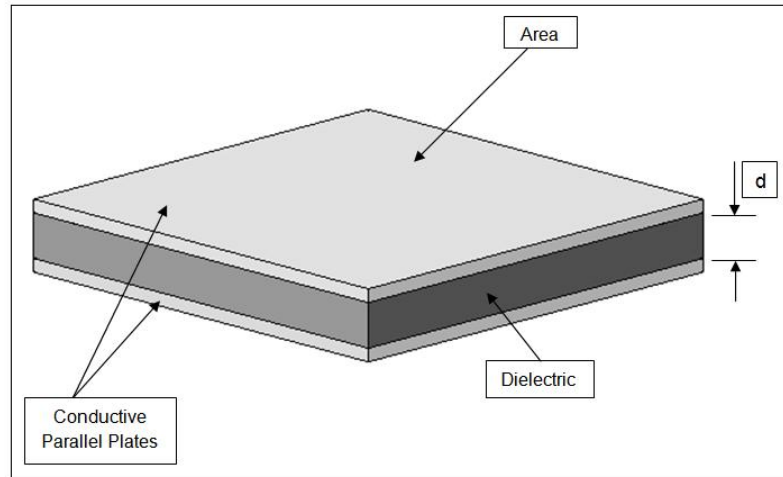


Figure 1–2: Schematic parallel plates pressure sensing element

1.2.3 Interdigital Pressure Sensor

The second battery-free wireless sensor proposed for pressure monitoring is an interdigital pressure sensor which has a interdigital capacitor connected to a inductor coil. These two components work together as an LC resonator whose resonant frequency is designed to change correspondingly with a change in the pressure that the sensor measures. The interdigital capacitor was built on a thick film which offers a planar multilayered structure, which can be embedded into laminate composite materials. No wire connection is needed for data acquisition and power supply, which makes the proposed sensor ideal for Structural Health Monitoring applications. The interdigital capacitor (IDC) was prepared on a thick flexible Pyralux



Figure 1–3: Schematic Interdigital Pressure sensor

film from DuPont. Figure 1-3 shows a schematic of proposed passive wireless pressure sensor.

The multi-layered structure of the sensor is also shown in the figure with the substrate and sensitive enhancement piezoelectric polymer above the conductive side of the interdigital capacitor. The sensor can be attached to any kind of material, and it is easy to embed into nonconductive material especially in laminated or dielectric materials. The frequency response of the sensor is remotely detected by monitoring the impedance across the terminals of the wide bandwidth reader antenna which actually also plays the role as a power transmitter by sending out oscillating magnetic field. A schematic view of the entire sensing system is shown in Figure 1-4.

1.3 Advantages Of Passive Wireless Sensing Technology

The technology developed in this research project will extend the basic knowledge of passive wireless sensing in the pressure sensing applications. The resulting sensor will offer many extraordinary features such as compact size, a contact-less

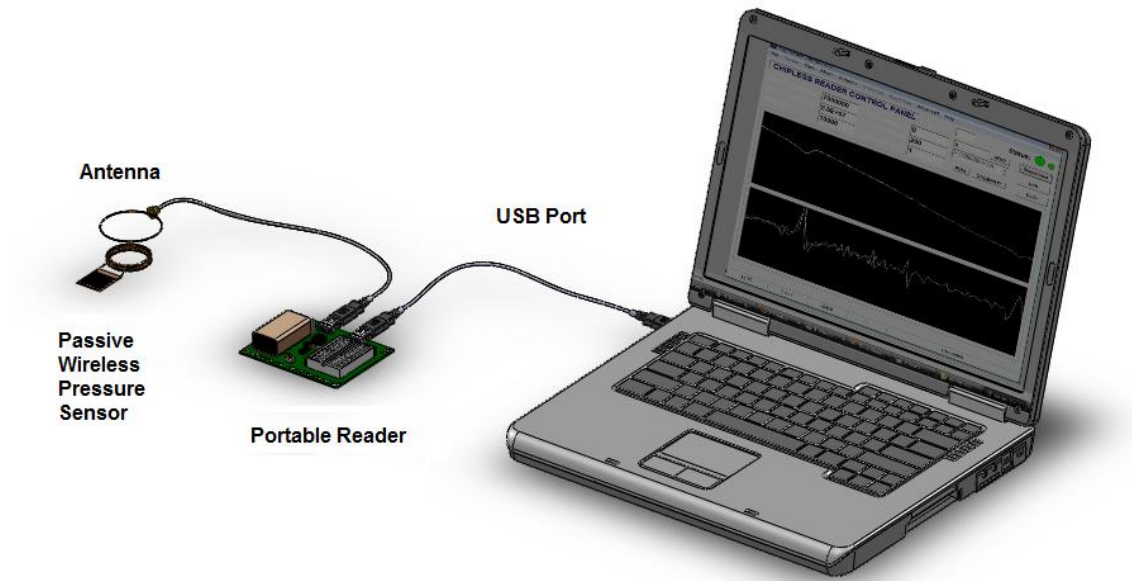


Figure 1–4: Proposed Wireless Pressure Sensing System

power supply, wireless data communication and and low cost. Meanwhile, no physical connections for power supply or data acquisition is required. Other advantages of the proposed wireless sensing system include:

- Remove physical contacts and electronics
- Create a capacitive frequency-encoded sensing mechanism based on LC circuit
- No wire is required to add new sensors

1.4 Research Objectives

The primary objective of this project is to conduct basic research on the passive wireless sensing mechanism in order to develop a novel passive wireless sensor to be used for measuring pressure. Particularly, the proposed project aims to accomplish:

1. Develop wireless sensing (platform) mechanism
2. Design two different capacitive pressure sensor designs
3. Sensors prototype fabrication
4. Sensors performance calibration and optimization

5. Demonstration of applications for the proposed sensor designs

1.5 Thesis Organization

The thesis consists of seven chapters. Chapter 2 is a review of the state-of-the-art pressure sensing technologies. Chapter 3 presents the design of a parallel plates capacitor, Interdigital capacitor and the spiral inductor, followed by a discussion on design principle for each component. Chapter 4 covers a sensor performance analysis with respect to resonant frequency, quality factor, coupling factor and the electric modeling for each proposed sensor. In Chapter 5 is presents the sensors prototype fabrication and experimental results. Finally, Chapter 6 summarizes the contributions of the work and the future improvements of the sensor technology. Developed programming codes in MATLAB and MATHEMATICA will be shown in Appendixes.

2

LITERATURE REVIEW

In recent years there has been an increasing interest in the use of wireless sensing technologies for Structural Health Monitoring (SHM) systems because they are being considered as substitutes for traditional tethered monitoring systems. Pressure sensing technology has become one of the most critical areas required for structural health monitoring (SHM). Pressure sensing systems, generally consist of certain calibrated transducers that converts a deformation or a mechanical movement into a pressure value output, such as Bourdon tubes, diaphragms, capsules, and bellows. This review is organized according to how the pressure effects are converted into other signals which can be processed. The purpose of this chapter is to outline actual pressure sensor sensing and the newly developed wireless sensing technology applied to pressure sensing. Advantages of our proposed sensors will be highlighted.

2.1 Traditional Pressure Sensing Devices

Mechanical elements such as plates, shells and tubes are used in order to sense pressure in the traditional pressure sensing devices; these elements are designed and constructed to be deformed when pressure is applied. This mechanism converts pressure to physical movement; later, this movement is transduced to obtain an electrical or other output. The sensing in traditional pressure sensing devices operation can be explained in functional blocks as is it described in the figure 2-1

Principal traditional sensing elements are Bourdon tubes, diaphragms, capsules, and bellows. Most of these types of devices, in order to increase their sensitivity, can

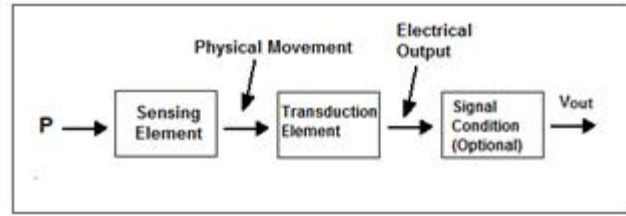


Figure 2–1: Typical pressure sensor’s functional blocks

be extended into spirals or helical coils. Some of these devices, like diaphragms, are used for operating electronic transducers which require less space and the motion that the devices produce is sufficient for the electronic applications and they are also available in a wide range of materials for corrosive service applications [17]. Most of these types of devices have large displacement which is useful in mechanical gauges and for electrical sensors that require a significant movement. Their principal disadvantages are that they require a power source in the transducer which converts the physical movement into electrical output and that they need wires for the operation.

2.2 Strain Gauge Pressure Sensors

In this kind of pressure sensor, the resistance of a wire filament, which is attached to a structure under strain, is measured. This device has problems with degradation of the bond between the wire filament and the diaphragm, and with hysteresis caused by thermoelastic strain in the wire [18]. The applications for this device which require remote sensing, monitoring, or recording are impractical and their mechanical linkages also limit their frequency response for dynamic pressure measurements. A strain gauge pressure sensor was developed by Gwilliam [19] for measuring tides on the continental shelf, this design uses a capacitor placed in parallel with one arm of the Wheatstone bridge and produces a phase shift in the state of bridge balance.

2.3 Potentiometric Pressure Sensors

The design of this device consists of a precision potentiometer, whose wiper arm is mechanically linked to a Bourdon or bellows element. A Wheatstone bridge circuit is used by the potentiometer for converting the deflection of the wiper arm into a resistance measurement. Errors into this type of measurement are introduced by the linkages connecting the wiper arm to the Bourdon tube, bellows, or diaphragm element. Temperature effects cause additional errors because of the differences in thermal expansion coefficients of the metallic components of the system. Errors will also develop due to mechanical wear of the components and of the contacts [20]. A Novel electrochemical Potentiometric Pressure Sensor was developed by Jan-Fong Jue [21], this design does not require a power source, has a temperature-independent signal, and can be used at temperatures over $400^{\circ}C$. Commercial applications for these low-cost pressure sensors include: geothermal drilling, oil drilling, monitoring pressure in chemical reactors, aviation, the automotive industry, and the measurement and monitoring of pressure in any high temperature (up to $700^{\circ}C$) application.

2.4 Resonant-Wire Pressure Sensors

In this kind of sensor, a wire is gripped by a sensing diaphragm at one end, and by the static member at the other. An oscillator circuit is used to produce the wire oscillation at its resonant frequency. The frequency of the wire changes in relation to the pressure, due to the change of the wire tension in relation with the pressure. The shift is detected by a digital counter. This type of transducer can be used for low differential pressure applications as well as to detect absolute and gauge pressures because the change in frequency can be detected precisely. The disadvantages of this type of sensor include sensitivity to temperature variation, a nonlinear output signal, and some sensitivity to shock and vibration[20].

2.5 Inductive Pressure Sensors.

Inductive pressure sensors are coupled with a diaphragm or a bourdon tube. A ferromagnetic core is attached to an elastic element and has primary and secondary windings. A current is charged to the primary winding. When the core is centered then the same voltage will be induced to the two secondary winding. If the core has a move with a pressure change, the voltage ratio between the two secondary windings changes. The difference between the voltages is proportional to the change in pressure. These may be used with any elastic element (though, it is typically coupled with a diaphragm or a bourdon tube). The pressure reading generated will be determined by voltage calibration. Thus, the range of pressure in which this sensor may be used is determined by an associated elastic element but falls in the range of 250 Pa - 70 MPa.

2.6 Piezoresistive Pressure Sensors

The piezoresistive pressure sensor consists of a silicon chip with an etched diaphragm and, a glass base anodically bonded to the silicon at the wafer level. The front side of the chip contains four ion-implanted resistors in a Wheatstone bridge configuration. The resistors are located on the silicon membrane and metal paths provide electrical connections. When a pressure is applied, the membrane deflects, the piezoresistors change unbalancing the bridge. Then a voltage is developed proportional to the applied pressure. Silicon piezoresistive sensors have been widely used for industrial and biomedical electronics. The piezoresistive sensors have excellent electrical and mechanical stability that can be fabricated in a very small size [20].

2.7 Strain Gauge Transducers

Strain gauge transducers are based on metal or silicon semiconductor strain gauges. The gauges can be discrete units attached to the surface of the strained element or unbonded gauges. The gauge material can be sputtered onto a diaphragm or diffused into a silicon diaphragm structure. The most common force-summing device for strain gauge transducers is the diaphragm, which may be flat or sculptured. Strain gauges are also used on bourdon tubes and bellows assemblies. Strain gauges are made of materials that exhibit significant resistance change when strained. This change is the sum of three effects. First, when the length of a conductor is changed, it undergoes a resistance change approximately proportional to change in length. Second, in accordance with the Poisson effect a change in the length of a conductor causes a change in its cross-sectional area and a resistance change that is approximately proportional to change in area. Third, the piezoresistive effect, a characteristic of the material, is a change in the bulk resistivity of a material when it is strained. All strain gauge materials exhibit these three properties, but the piezoresistive effect varies widely for different materials. Metal strain gauges are networks of wire or patterns of thin metal foil fabricated onto or into a backing material and covered with a protective film.

2.8 Capacitive Pressure Sensors

Capacitive pressure sensors typically use a thin diaphragm as one plate of a capacitor. Applied pressure causes the diaphragm to deflect and the capacitance change. This change of capacitance is either used to vary the frequency of an oscillator or is detected by a bridge circuit. This change may or may not be linear and is typically on the order of several picofarads out of a total capacitance of 50-100 pF. The change in capacitance may be used to control the frequency of an oscillator or to vary the coupling of an AC signal through a network. The primary advantages

are low hysteresis, good linearity, stability, and repeatability, static pressure measurement capability, and a quasi-digital output. For capacitive pressure sensors the capacitance is given by the equation:

$$C = \frac{\varepsilon_0 \varepsilon_r A}{d} \quad (2.1)$$

Where ε_0 is the air permittivity, ε_r is the relative permittivity of the material between the plates or inside the diaphragm, A is the area of the plates of diaphragm and d is the distance between plates or diaphragm.

Nowadays Micro-scaled Pressure sensor have applications in areas such as automotive systems, industrial control, environmental monitoring and biomedical diagnostics. Most of capacitive pressure sensors generally operate by sensing the displacement of a thin, flexible conductive membrane as one of the electrodes, while the other electrode is fixed beneath the membrane. Deformation of the movable part due to applied pressure is sensed and translated into an electrical capacitance change [22]. Several researchers have worked with capacitive pressure sensor using micro fabrication and/or mems fabrication [23–25] some examples are:

A micro capacitive pressure sensor was developed by Chia-Chu Chiang et al [10] for biomedical applications. This design can be embedded into the cuff electrode for in situ monitoring of the interface pressure between implanted cuff and nerve tissue. The structure of this capacitive pressure sensor consists of two parallel conductive plates, one dielectric layer sandwiched between the two conductive plates, and two outer insulating layers. Polyimide and PDMS were the materials chosen as the material of the insulating layer and the material of the dielectric layer, respectively. The sensor is mainly fabricated by surface micromachining techniques.

S.T. Moe et al [26] developed a capacitive differential pressure sensor for the pressure range of 0 – 1 bar, the primary field of application is hydrodynamic flow

measurements in hot petroleum wells. The design of this capacitive pressure sensor consists of a stack of fusion-bonded silicon wafers, then a bossed diaphragm etched in the upper wafer bends due to the differential pressure across it. A reference capacitor insensitive to the differential pressure enables compensation for capacitance shifts caused by ambient pressure and temperature changes. This design uses a powered device for signal read-out.

2.9 Wireless Sensing Technology

In this section will be discussed the actual wireless sensing technology for Structural Health Monitoring and some examples applied to pressure sensing.

2.9.1 Commercial Wireless Sensor Platforms

Commercial wireless sensor platforms have emerged in recent years in SHM applications and their principal advantages include immediate out-of-the-box operation, availability of technical support from the platform manufacturer, and low unit costs. These advantages produce that commercial wireless sensor platforms are widely used by many academic and industrial research teams within SHM systems. A major reason for the commercial wireless sensor platforms' popularity is the fact that some of these devices have open source design to the public, for example the Mote wireless sensor platform initially developed at the University of California-Berkeley and subsequently commercialized by Crossbow (<http://www.xbow.com/>). Other electronics companies such as Ember (<http://www.ember.com/>), Microstrain (<http://www.microstrain.com/>), and Sensametrics (<http://www.sensametrics.com/>) have developed commercial wireless sensor platforms for SHM; in contrast to the Motes, these wireless sensor platforms are proprietary and not open source. Most of the commercial wireless platforms are active and require power source besides data acquisition and processing units.

2.9.2 Radio Frequency Identification Based Sensors

Life expectancy of portable power sources is one of the problems for the current wireless sensor technology due current battery technology only offers operational lives for a short time or for a long time with high costs. Many researchers in the wireless sensing technology have proposed one approach to solve this issue, employing radio frequency (RFID) wireless technologies for booth the delivery of power to wireless sensors as well as for data communication. The RFID-based wireless sensor captures the delivered energy and stores it in temporary capacitive storage elements in order to operate an ultralow-power sensor circuit [27]. Later the data are collected by the sensor; the stored power is used to modulate the sensor data on a radio frequency signal readable by the remote interrogator. The advantage of these battery-free wireless sensor technology is that they can operate indefinitely in the field.

Many researchers have proposed and developed battery- free wireless sensor technologies for SHM using RFID technology. Novak et al [28] have proposed the design of a novel wireless sensor for SHM, the main objective is to identify two possible damage states in civil structures: cracking in welded steel connections and corrosion in reinforced concrete elements. This design utilizes an inductor-capacitor (LC) circuit to allow a remote wireless reader to power the sensor and to receive measurement data. The characteristic of frequency of the LC circuit serves as the primary readout mechanism. Carkhuff and Cain [29] have proposed a passive RFID based wireless sensor to monitor concrete bridge decks for corrosion. This design adopts two inductive coils. One coil, tuned to 1 MHz, is to pick up power from a remote interrogator, while a second coil, tuned to 10.5 MHz, is for radio communication. Saafi and Romine [30] have proposed a novel design of a passive RFID-based corrosion sensor designed to be embedded into concrete during construction; this

design used the MEMS fabrication processes to enhance the sensitivity within the RFID-based corrosion sensor platform. This sensor is capable of sensing environmental parameters within concrete bridge decks such as the pH, relative humidity, and the concentration of chloride ions and CO₂. The principal disadvantage of Passive RFID-based technologies only offer short communication ranges ($< 5m$) between the reader and the device. This range can be drastically reduced when the sensor is embedded in structural materials. Munnangi *et al.*[31] proposed a cantilever based capacitive pressure sensor for detecting the heartbeat signal. This pressure sensor has simple design with only few process steps compatible to standard CMOS flow was proposed. The sensor was integrated with the other blocks of RFID tag and the entire circuit was verified by simulation.

Tire-pressure monitoring system (TPMS) which is an electronic system designed to monitor the air pressure inside all the pneumatic tires on automobiles, airplane undercarriage, straddle-lift carriers, forklifts and other vehicles; is another application of RFID sensing technology applied to pressure measurement. Commercial TPMS have been developed by companies such as Royal Philips Electronics, in this design an RFID chip that can be bonded inside a tire, and read remotely by antennas installed in the wheel hubs of the car. As there is no physical link, reliable interaction with the tag is possible even while in motion. This RFID application solves a challenging problem because the tires are spinning and sensors can only be connected by wires if concentric connection rings are engineered around each wheel axial, making the engineering complicated and costly [32]. The figure 2-2 [32] is shows a schematic view of the TPMS in a car.

2.9.3 Wireless SAW Sensors

In the recent years have been developed wireless measurement systems with passive surface acoustic wave (SAW) sensors for several physical quantities [33, 34].

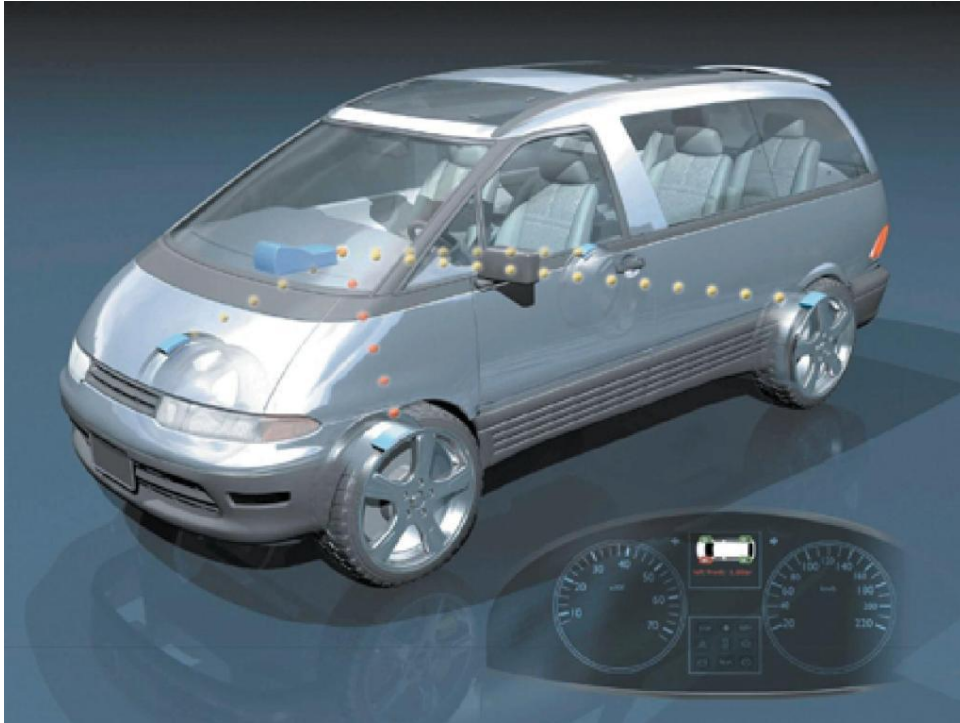


Figure 2-2: Car tire incorporating RFID pressure sensor readable from the car

Principal features of SAW sensor systems are a large readout distance and an energy supply of the sensor only by the electromagnetic RF field of the transceiver unit. A prototype of a tire pressure sensor unit with a typical accuracy of 15 kPa within a pressure range of 100 to 400 kPa, was proposed by Schimetta et al [35], and the design used the combination of a SAW transponder tag with a high-Q capacitive pressure sensors to "SAW hybrid sensors". This kind of passive devices re-transmit a linearly distorted version of the radio request signal. The distortion is affected by the measurand. The energy of the RF radio signal is stored in the SAW, which yields the required time delay between request signal and sensor response for TDD [36].

2.9.4 RF Powered LC Sensors

The RF powered LC sensors are capable of eliminating the need for onboard power and exposed interconnections. These kinds of sensor use a wireless telemetry

system which consists of an LC resonant sensor, and an external transmitter/receiver loop antenna. The interaction between the external antenna and the sensor is explained via the equivalent circuit model. When another coil is placed in the near region of the external coil, as a result of coupling between both coils, it is possible to detect its resonant frequency from the input impedance measurements of the external antenna. The small size and stable characterization make them popular in various harsh environment measurement applications like pressure sensors, some examples of these applications are:

An absolute wireless pressure sensor that consists of a capacitive sensor and a gold-electroplated planar coil was developed by Akar et al [37]. The design of this pressure sensor includes a thin silicon diaphragm, when the pressure is applied to the sensor, the thin diaphragm is deformed changing the capacitance formed between it and a metal electrode supported on a glass substrate. The resonant frequency of the LC circuit formed by the capacitor and the inductor changes as the capacitance changes; this change is sensed remotely through inductive coupling, eliminating the need for wire connection or implanted telemetry circuits. The fabrication process of the wireless capacitive pressure sensor is based on the bulk silicon dissolved wafer process with some additional steps needed to integrate the on-chip electroplated coil, the fabricated devices measure $2.6\text{mm} \times 1.6\text{mm}^2$ in size and are optimized to provide a dynamic range of 0 – 50 mmHg.

Fonseca et al [38] developed a passive ceramic pressure sensor that uses a wireless telemetry scheme. The sensor's design contains a passive LC resonator comprised of a movable diaphragm capacitor and a fixed inductor, thereby causing the sensor resonant frequency to be pressure-dependent. In this research the data was retrieved with an external loop antenna and the sensor has been fabricated, characterized and compared with an electromechanical model. It was operated up to 400 C in a pressure range from 0 to 7 Bar.

Nabipoor developed a passive telemetry LC absolute pressure and temperature sensor to be used in a Tire Pressure Monitoring System (TPMS)[39]. The design of this device consists in a passive telemetry LC pressure and temperature sensor a pressure sensitive capacitor which is used in parallel with a temperature sensitive inductor and together they make a LC tank circuit. Changing the applied pressure affects the resonant frequency of the circuit while the temperature affects the bandwidth and amplitude of the impedance at this frequency. The fabrication of this device included : Bottom electrode of the capacitor and the coil of the inductor are fabricated on a glass wafer. The capacitor top electrode is created in a $5\mu\text{m}$ square recess in silicon, the figure 2-2 [39] shows a.

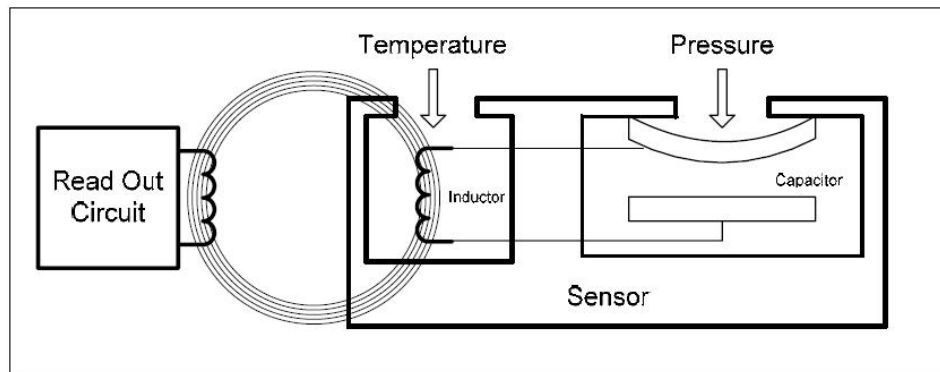


Figure 2–3: The working principle of the LC pressure and temperature sensor

A passive wireless pressure sensor for applications that require mechanical robustness was developed by Takahata [40]. The design of this sensor consists in two micromachined metal plates and an intermediate polymer layer that is soft enough to deform in a target pressure forming the capacitor. A passive inductor-capacitor circuit tanks was fabricated by combining the capacitive sensor with an inductive coil in order to do the interrogation of the resonant frequency of the circuit. In this thesis two RF powered LC pressure sensor will be developed. These sensor employ a parallel plate and an interdigital capacitor each one, connected to a inductor coil to form an inductor capacitor (LC) resonator circuit. This resonant wireless platform

removes any electronic components or physical contacts.

2.10 Conclusions

The majority of commercially available pressure sensors are actually made mechanical elements such as plates, shells and tubes. These technologies have been used for several decades; they are inexpensive, use wires and power source for their operation. However, those commonly used traditional techniques are difficult to apply for measurements in hostile environments, e.g., rotating components, places with difficult access, applications where is need do not use wires and power source. Due to its, compact size, a contact-less power supply, wireless data communication, and low cost, RF powered LC sensing technology will be chosen in this research project to develop a pressure sensor.

3

BATTERY-FREE WIRELESS PRESSURE SENSOR DESIGN

This chapter starts with the design principle of the proposed pressure sensors. In this sensor, the energy transfer of the resonant circuit is based on the interaction between the inductor in the sensor and the reader antenna. Modeling and calculations of the capacitors and the coil inductor are also discussed in order to determine the resonant frequency. Electrical modeling of the resonant circuit is built to simulate resonant frequency variations in response to pressure.

3.1 Parallel Plate Capacitor

A capacitor is a device that stores electric charge. Capacitors vary in shape and size, but the basic configuration is two conductors carrying equal but opposite charges. The simplest example of a capacitor consists of two conducting plates of area A , which are parallel to each other, and separated by a distance d , as shown in Figure 3-1.

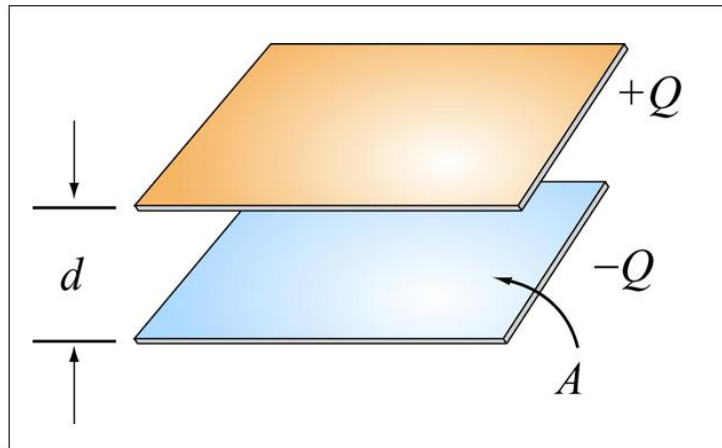


Figure 3-1: A parallel-plate capacitor

The amount of charge Q stored in a capacitor is linearly proportional to, the electric potential difference between the plates. Then,

$$Q = C |\Delta V| \quad (3.1)$$

Where C is a positive proportionality constant called capacitance. Physically, capacitance is a measure of the capacity of storing electric charge for a given potential difference $|\Delta V|$. In order to get the expression for the capacitance in systems with simple geometry, let consider consider two metallic plates of equal area A separated by a distance d , as shown in Figure 3-2. The top plate carries a charge $+Q$ while the bottom plate carries a charge $-Q$ [41].

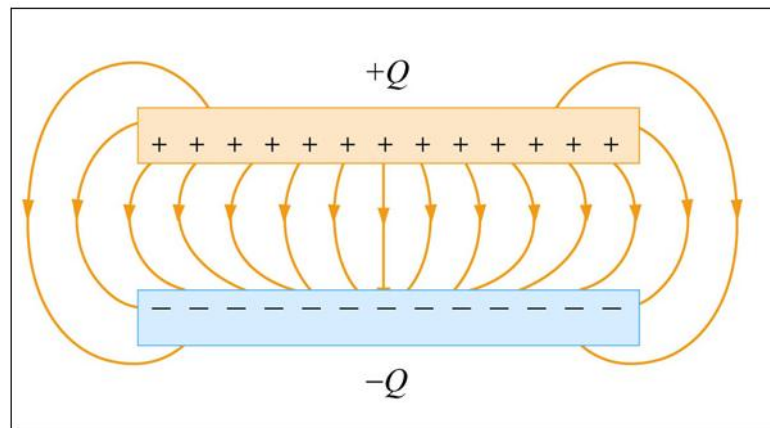


Figure 3-2: The electric field between the plates of a parallel-plate capacitor

A real capacitor has a finite size. Thus, the electric field lines at the edge of the plates are not straight lines, and the field is not contained entirely between the plates. This is known as edge effects, and the non-uniform fields near the edge are called the fringing fields. In Figure 3-2 the field lines are drawn by taking into consideration edge effects. However, the field lines between the plates will be considered straight lines for assuming an idealized situation. In the limit where the plates are infinitely large, the system has planar symmetry and we can calculate the electric field everywhere using Gauss's law. The voltage is defined as the line integral of the

electric field between the plates

$$V = \int_0^d E dz = \int_0^d \frac{\rho}{\varepsilon} dz = \frac{\rho d}{\varepsilon} = \frac{Qd}{\varepsilon A}. \quad (3.2)$$

Solving this for $C = Q/V$ reveals that capacitance increases with area and decreases with separation

$$C = \frac{\varepsilon A}{d}. \quad (3.3)$$

3.1.1 Parallel Plate Sensor Design

The change of capacitance in the parallel plate sensing element is due to the deformation of a polymeric dielectric material between the two conductive parallel plates. When a pressure is applied on the sensor, the distance between two sensing electrodes is reduced and the capacitance arises accordingly the pressure, as is shown in the figure 3-3. The materials used for the parallel plates for the intermediate polymer layer were room-temperature-vulcanizing (RTV) liquid rubber of polyurethane and Polydimethylsiloxane (PDMS). The liquid rubber of polyurethane offers mechanical robustness such as high tear and abrasive resistances, chemical resistance and controllability of its softness over a wide range. The PDMS is a commercially type of silicone rubber with a wide range of applications and good mechanical properties for sensor applications [42, 43] for instance (interconnection layer between two silicon wafers, spring material in acceletometers and top elastomer on tactile sensors and biosensors). In this work are compared these two materials for use in parallel plate pressure sensors. The capacitance between two parallel electric conductive plates can be written as,

$$C = \frac{\epsilon_0 \epsilon_r A}{d} \quad (3.4)$$

Where ϵ_0 is the air permittivity ($8.854 \times 10^{-12} F/m$), ϵ_r is the relative permittivity of the material between the plates or inside the diaphragm, A is the area of the plates of diaphragm and d is the distance between plates or diaphragm.

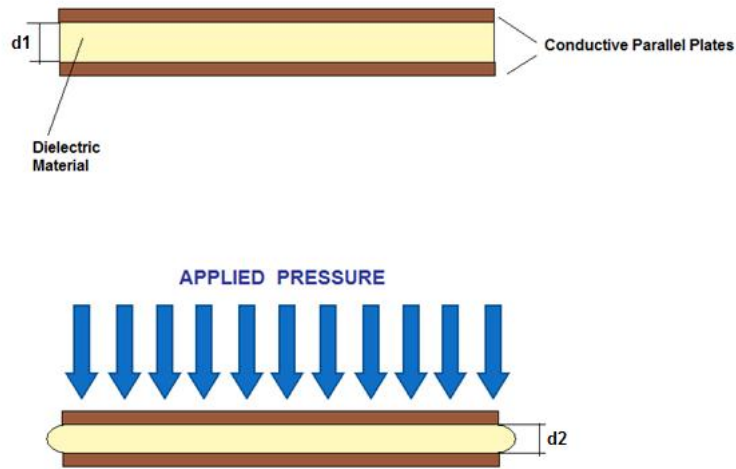


Figure 3–3: Schematic view of the parallel pressure sensor when is applied a pressure

The permittivity of the polyurethane is reported to be stable over the pressure range that is involved in this research (0-300Kpa) [44] and experimentally was found the value of 4.33 [40] and the other hand the permittivity of the PDMS is 2.65 [10] thus the capacitance change is a function of the distance between the metallic parallel plates. With these, the ratio of the resonant frequency after the compression to the original distance is:

$$\left(\frac{f}{f_0}\right)^2 = (C_o/C) = (d/d_0) \quad (3.5)$$

Where C_o, f_0 and d_0 are the original capacitance, frequency and distance prior to the compression respectively. The relationship between the applied pressure and the ratio in the resonant frequency, $f/f_0 = F$, for a rectangular layer of and incompressible, homogeneous elastomer that is bonded with rigid plates on both sides can be expressed [40] as:

$$P = \frac{EAS_0^2}{2} \left(\frac{1}{F^4} - 1 \right) - E \left[1 + \frac{1}{3} \left(\frac{Y^2 - W^2}{Y^2 + W^2} \right)^2 \right] \log(F^2) \quad (3.6)$$

Where E is the young modulus of the rubber, 2Y and 2W are the length and width of the rectangle layer, respectively, A is a Constant given by:

$$A = \frac{4}{3} + \frac{W}{Y} \left(2 - \frac{11W}{10Y} \right) \quad (3.7)$$

And S is a shape factor:

$$S = \frac{YW}{2T(Y + W)} \quad (3.8)$$

Where 2T is the thickness of the layer between the parallel plates and S_o is the original shape factor with the initial thickness $2T_0$ before compression. The young's modulus for the polyurethane was experimentally found in [40] with a value of 67Kpa and the value of young's modulus for PDMS is 750Kpa[45].

The measure of the prototypes designed and fabricate the measures of the parallel plates are: 25mm x 40mm and thickness of the dielectric layer is 1.3mm for each dielectric material. Each device was coupled with an circular inductive coil, the coil was formed by winding (7 turns) of coated copper wire AWG 23($\varphi 0.6mm$), forming a circular loop (40mm dia) Using the formulas to get an approximation of Inductance for a circular loop [46], the inductance obtained is equal to $5.57\mu H$. The design of

the L-C circuit tank shown in the figure 3-4 has a theoretical nominal capacitance for the polyurethane dielectric material of 29.3 pF and a nominal capacitance of 17.9pF for the PDMS dielectric material. The nominal resonant frequencies for the Polyurethane device and PDMS device are 12.44 Mhz and 15.91 Mhz respectively. The table 3-1 shows a summarizing of design parameters for each sensor

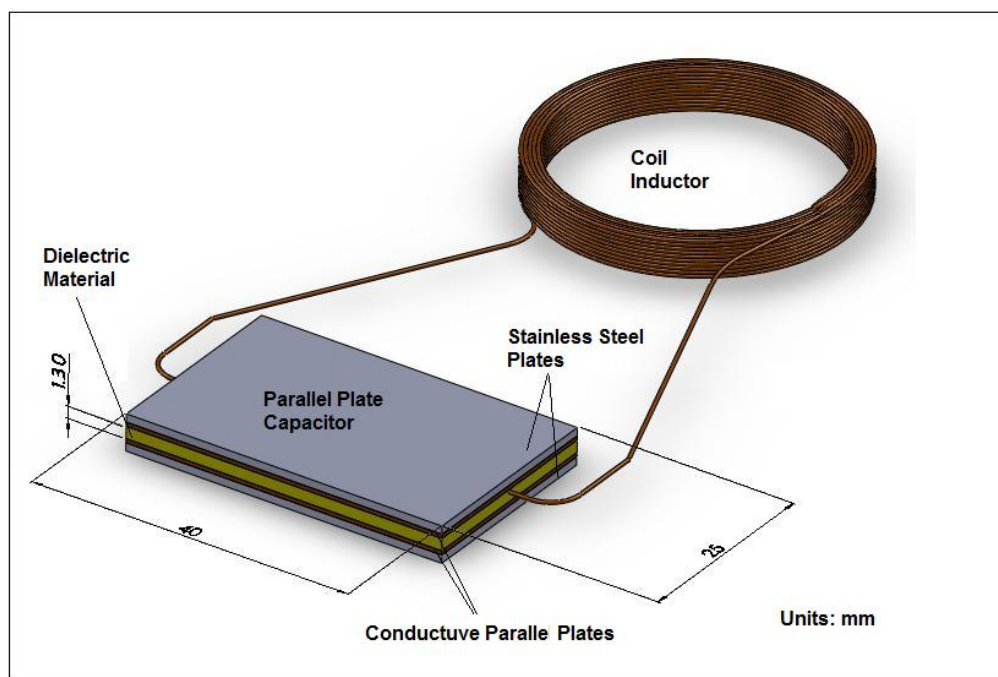


Figure 3-4: Parallel plate pressure sensor design

Table 3–1: Electrical Parameter Values

DESIGN PARAMETER	Polyurethane	PDMS
Length	40 mm	40mm
Width	25 mm	25mm
Thickness dielectric	1.3 mm	1.3 mm
Young Modulus	67Kpa	750Kpa
Relative Permittivity	4.33	2.65
Sensor Nominal Capacitance	29.3 pF	17.9 pF
Sensor Inductance	5.57 μ H	5.57 μ H

3.2 Interdigital Capacitor

This section starts with the construction of the proposed passive pressure sensor and the physical model of the interdigital capacitor as the pressure sensing element. After the exploration of the geometry dependent capacitance of the interdigital capacitor, the pressure sensing principles of the interdigital electrodes are disclosed and exhaustively explained. Aiming to have minimized size and improved sensitivity, design considerations of the geometric dimensions of the interdigital capacitor are discussed.

InterDigital Capacitive (IDC) sensors are perhaps one of the most promising devices in terms of fabrication costs and ease of integration in a standard complementary metal-oxide silicon process, requiring only minimum post-processing[47] and nowadays advances in such fields as nondestructive testing (NDT), microelectromechanical systems (MEMS), telecommunications, chemical sensing, piezoelectrics, and biotechnology involve interdigital electrodes in very different ways. Planar interdigitated array electrodes are also have many applications such as complex

permittivity characterization of materials [48], gas detection [49], determining components in aqueous solutions [50], estimation of fiber, moisture and titanium dioxide in paper pulp[51] etc. The operating principle behind the interdigital sensor is very similar to the one observed in a parallel plate capacitor; figure 3-5 shows the relationship between a parallel plate capacitor and an interdigital sensor, and how the transition occurs from the capacitor to a sensor. There is an electric field between the positive and negative electrodes and figure 3-5 a, b and c shows how these fields pass through the material under test (MUT). Thus material dielectric properties as well as the electrode and material geometry affect the capacitance and the conductance between the two electrodes.

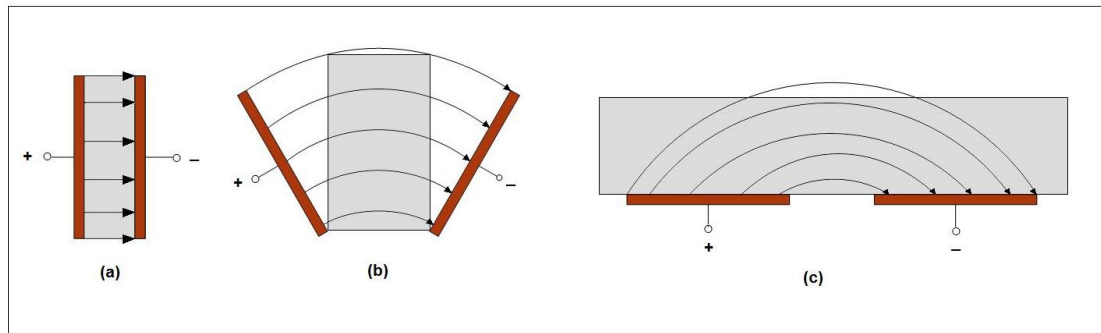


Figure 3-5: Operating principle of interdigital sensor

A schematic description of the repeating geometry of the IDEs sensing element is shown in the figure 3-6, the IDEs consist two series of electrodes with opposite polarities positive (+) and negative (-) on each finger. An application of a differential voltage across the two electrode terminals is involved in the operation of the IDC. The voltage on each individual IDE fingers connected to the same terminal keeps continuously constant due to electrostatic at some specific time moment. Symmetry property in the IDC and helps to disassemble the overall system into repeating cells with identically the same physical behavior were revealed on investigations of the potential field in the system geometry. The analysis of the IDC is simplified ignoring the parasitic influence on the IDEs finger edges and ends. A single IDE

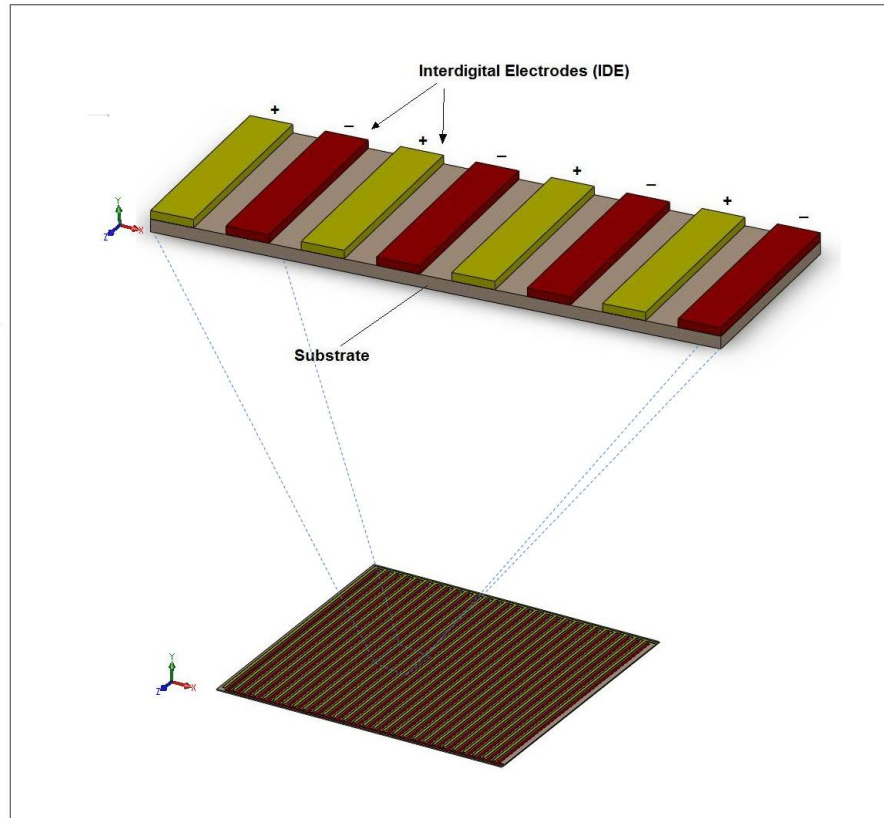


Figure 3–6: A schematic view of the interdigital capacitor simplification.

in x-direction is broken up into two parts in the middle of the finger along the z-coordinate. This half-finger corresponds to the other half-finger on the opposite IDE; under this assumption, the entire IDC is predigested into a single half-unit cell as a straightforward model. However, this is still a 3-D problem for electrical field. Without varying material properties along z-direction, the IDC unit cell model will be 2 dimensional which possesses only x- and y-direction. In each of these repeating 2-D unit cell in IDC, the electric field, the piezoelectric polarization field and the capacitance can be treated the same. Thus, analysis of the electrostatic properties of this 2-D unit cell is critical for the determination of the electrostatic properties of the entire IDC [52].

3.2.1 Interdigital Capacitance Analysis

Even 2-D approximation of the interdigital structures results in the electric field distribution that is too complex to be described rigorously by simple algebraic expressions. The potential distribution along the sensor-material interface between the two ports is not known in advance, and depends on the material properties and geometric parameters of the structure. A useful approach for the calculation of 2D interdigital electrode capacitance stems from conformal mapping. Conformal mapping is one of the most frequently used approaches to transform an appropriate space region of IDC to a parallel plate capacitor geometry whose capacitance value can be calculated. Igreja [53] developed an analysis and analytical solutions for IDC capacitance using conformal mapping.

The geometric dimensions of the IDC are indicated in figure 3-7, this figure shows a 2-dimensional cross-sectional view of the IDC with all the geometric dimensions and dielectric properties notified, where t is the thickness of the IDEs, h is the thickness and ϵ_r is the permittivity of the substrate. The gaps between electrodes have a width of g_c and the fingers have a width of w_c . All the fingers are connected to two common comb electrodes. Each comb electrode has a number of finger of length L_c and is connected to each end of the spiral inductor. The wavelength is calculated $\lambda = 2(g_c + w_c)$. The dimensional parameter which the capacitance also depends on is called metal ratio and is calculated as $\eta = w_c/(g_c + w_c) = 2w_c/\lambda$

The proposed Battery-Free Interdigital pressure sensor will be mounted between two layers of polyethylene with 3mm of thickness each one; avoiding the presence of metal near to the IDC. The schematic view of the IDC on the test machine is shown in the figure 3-8.

By symmetry, the perpendicular planes halfway between the electrodes are equipotential planes with $V=0$ which acts like an electric ground where electric field lines

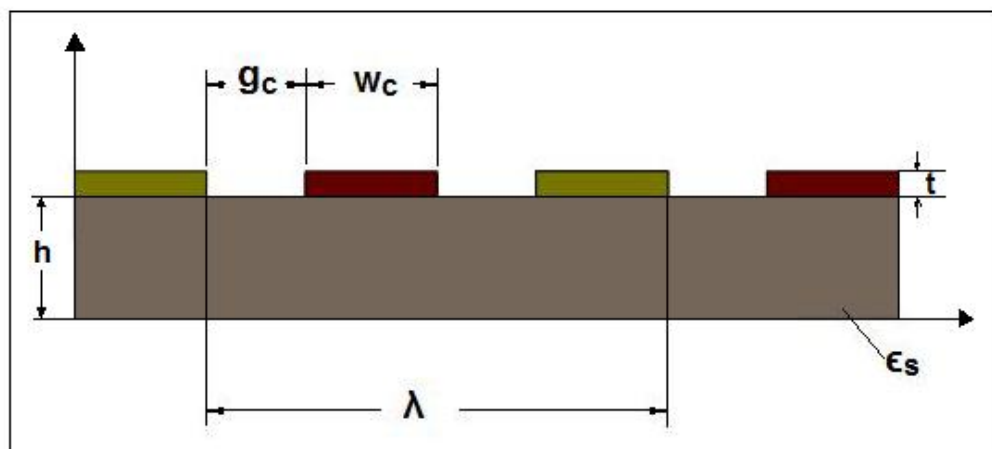


Figure 3-7: 2-dimensional cross-sectional view of the IDC with the geometric dimensions

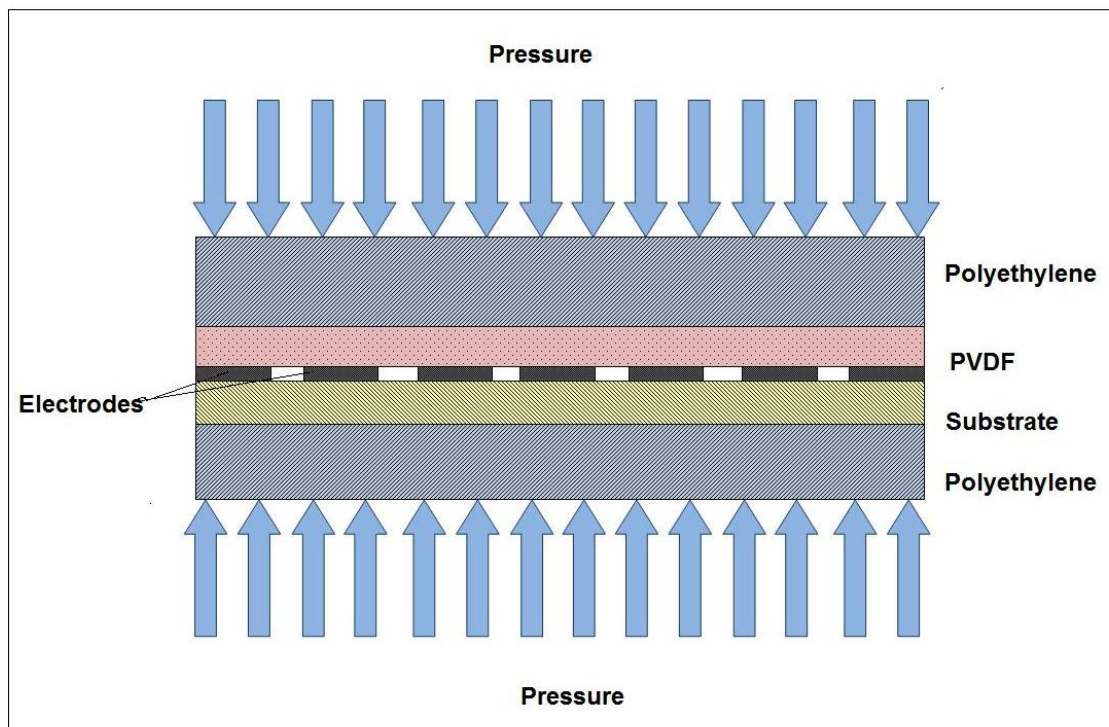


Figure 3-8: Schematic view of the IDC on the test machine

crossing normal to these planes shown in Figure 3-9. This holds exactly true for an infinite periodic structure whose electrodes fingers have an infinite length. In the case of a finite periodic structure, there is an error incurred by this assumption due to impacts from other cells and thus the variation in the ground planes, which especially happen closer to the boundary electrodes. Therefore, it is assumed that most of the polarization phenomena occur in a region where the variation in the ground planes is not significant. The finite length of the electrodes is much greater than the wavelength of the IDC structure so that for practical purpose they can be considered as infinity [52]. Can also be neglect, the capacitance at the side walls of the electrodes, because the thickness of the electrodes are much thinner than their width, and thus, the capacitance is specified between the upper and lower half planes. However, the thickness of the thicker electrodes in our design can not be ignored. Corrections to the equations derived by Igreja are added taking into the account of electrode thickness seen in Equations 3.9 and 3.10.

At the lower half plane of the IDC, the thickness of the substrate ($\approx 18\mu m$) is not much smaller than the wavelength of the IDC so that the substrate can be considered as a finite layer. Since the thickness of the polyethylene layers ($\approx 3mm$) is much greater than the wavelength, and thus the thickness of the polyethylene layers are considered as an infinite layer. At the upper half plane, the pressure sensitive layer is considered as finite layer. The calculation of either the CI or CE can be done based on this half unit cell model as is shown in the figure 3-9.

The total capacitance of the half unit cell CI and CE can be treated as a summation of four individual capacitances which are given below:

$$C_I = C_{I_{Poly\infty}} + C_{I_{PDVF}} + C_{I_{substrate}} + C_{I_{Poly\infty}} \quad (3.9)$$

$$C_E = C_{E_{Poly\infty}} + C_{E_{PDVF}} + C_{E_{substrate}} + C_{E_{Poly\infty}} \quad (3.10)$$

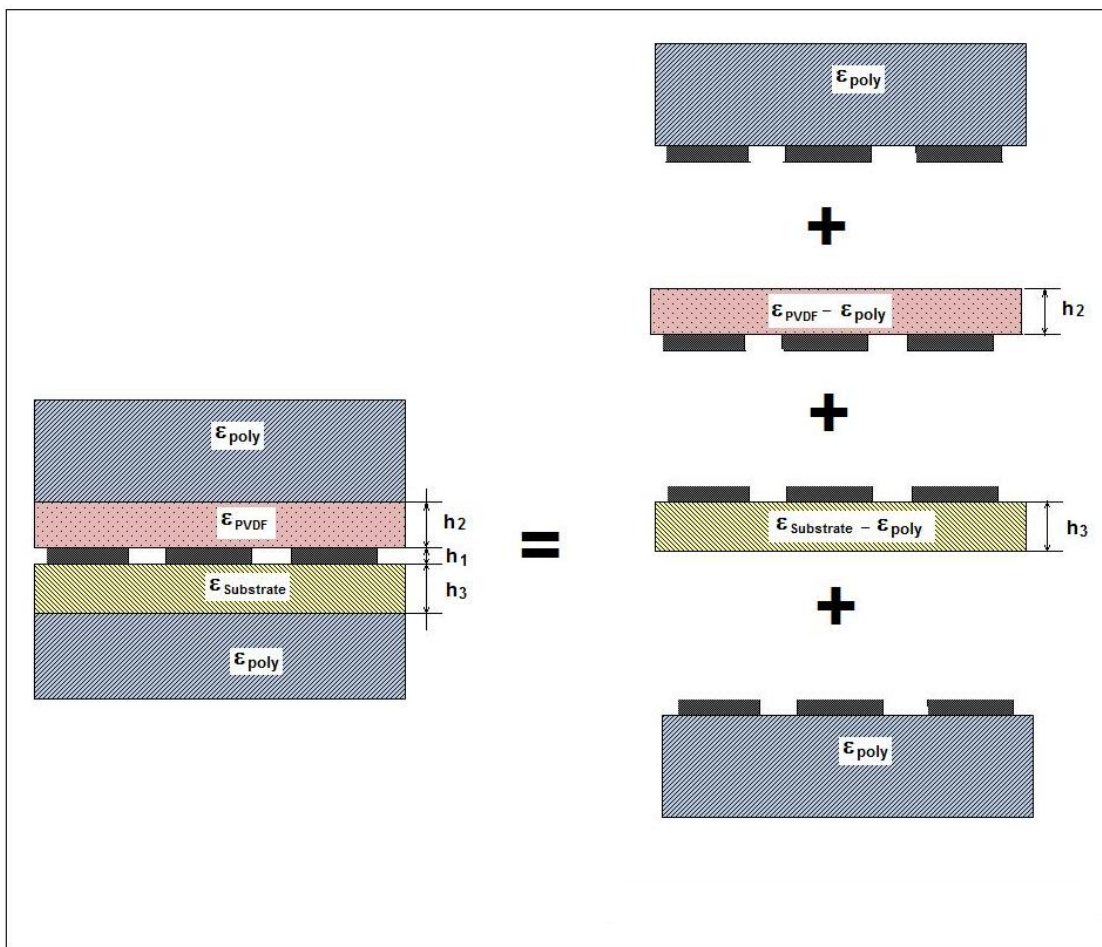


Figure 3-11: Splitting of the proposed three-layered IDC

Table 3–2: Detailed equations needed for the calculation of CI and CE for a finite layer as well as for an infinite layers

	Interior Electrodes	Exterior Electrodes
Finite Layer	$C_I = \varepsilon_0 \varepsilon_r \frac{K(k_I)}{K(k'_I)}$ $K'_I = \sqrt{1 - k_I^2}$ $k_I = t_2 \sqrt{\frac{t_4^2 - 1}{t_4^2 - t_2^2}}$ $t_2 = \operatorname{sn}(K(k)\eta, k)$ $t_4 = \frac{1}{k}$ $k = \left(\frac{v_2(0, q)}{v_3(0, q)} \right)^2$ $q = \exp(-4\pi r)$	$C_E = \varepsilon_0 \varepsilon_r \frac{K(k_E)}{K(k'_E)}$ $K'_E = \sqrt{1 - k_E^2}$ $k_E = \frac{1}{t_3} \sqrt{\frac{t_4^2 - t_3^2}{t_4^2 - 1}}$ $t_3 = \operatorname{cos} h \left(\frac{\pi(1-\eta)}{8r} \right)$ $t_4 = \operatorname{cos} h \left(\frac{\pi(\eta+1)}{8r} \right)$ $\eta = \frac{g_c}{g_c + w_c} = \frac{2g_c}{\lambda}$ $r = \frac{h}{\lambda}$
Infinite Layer	$C_I = \varepsilon_0 \varepsilon_r \frac{K(k_{I\infty})}{K(k'_{I\infty})}$ $K_{I\infty} = \operatorname{sin} \left(\frac{\pi}{2} \eta \right)$	$C_E = \varepsilon_0 \varepsilon_r \frac{K(k_{E\infty})}{K(k'_{E\infty})}$ $K_{E\infty} = \frac{2\sqrt{\eta}}{1+\eta}$

complete elliptic integral of the first kind with modulus k, k' is the complementary modulus of k , v_2 and v_3 are the Elliptic theta functions, $sn(z, k)$ is the Jacobi elliptic function of modulus k , $\lambda = 2(gc+wc)$ is the spatial wavelength, and the adimensional parameter which the capacitance of the IDC depends on is the metal ratio which can be calculated as $\eta = wc/(gc + wc) = 2wc/\lambda$, $r = h/\lambda$ where h is the thickness of the dielectric layer and ε_0 is the permittivity of free space. The above equations are written for the case of a thick substrate (the thickness of the substrate must be much higher than $\lambda/2$ if we want to consider it like a infinite layer).

In conclusion, the total capacitance is a function of two adimensional parameters, η (metallization ratio) and r (Layer thickness to wavelength ratio), length and number of electrodes, height of sensing layer and as well as the dielectric permittivity of each layer (substrate, protective layers and sensing layer) $C = C(\eta, r, \varepsilon_s, \varepsilon_{PVDF}, \varepsilon_{Poly}, h_2, h_3, l, N)$.

The general expressions used for the estimation of multilayer inter-digital electrode capacitance can be found in literature [53]. It is of the form, The total capacitance of a IDC-S is given by:

$$C_{IDC} = (N - 3) \frac{C_{I,IDC}}{2} + 2 \frac{C_{I,IDC} C_{E,IDC}}{C_{I,IDC} + C_{E,IDC}} \quad (3.11)$$

Where $C_{I,IDC}$ and $C_{E,IDC}$ are developed using the equations and the partial capacitance technique [53]. A IDC-S with a thick substrate of relative permittivity ε_s , one sensitive layer of relative permittivity ε_1 , and the infinite protective layer of relative permittivity ε_p will have their total capacitances $C_{I,IDC}$ (Interior electrodes capacitance) and $C_{E,IDC}$ (Exterior electrodes capacitance), using the connotation shown in the figure 3-11 and equations 3.9 and 3.10 we have: given by:

$$C_{I,IDC} = C_{I,Poly\infty} + C_{I,PVDF} + C_{I,S} + C_{I,Poly\infty} \quad (3.12)$$

$$C_{E,IDC} = C_{E,Poly\infty} + C_{E,PVDF} + C_{E,S} + C_{E,Poly\infty} \quad (3.13)$$

$$C_{I,IDC} = \varepsilon_0 L \left[2\varepsilon_{poly} \frac{K(k_{poly\infty})}{K(k'_{poly\infty})} + (\varepsilon_{PVDF} - \varepsilon_{poly}) \frac{K(k_{I,PVDF})}{K(k'_{I,PVDF})} + (\varepsilon_S - \varepsilon_{poly}) \frac{K(k_{I,S})}{K(k'_{I,S})} \right] \quad (3.14)$$

$$C_{E,IDC} = \varepsilon_0 L \left[2\varepsilon_{poly} \frac{K(k_{poly\infty})}{K(k'_{poly\infty})} + (\varepsilon_{PVDF} - \varepsilon_{poly}) \frac{K(k_{E,PVDF})}{K(k'_{E,PVDF})} + (\varepsilon_S - \varepsilon_{poly}) \frac{K(k_{E,S})}{K(k'_{E,S})} \right] \quad (3.15)$$

3.2.2 Geometry Dependent IDC Capacitance

Because of this geometry dependent capacitance in the interdigital capacitor, the design considerations are highlighted in this part. Effect of η on the value of capacitance is studied. Plot of the capacitance of different unit cell geometries indicate the variation of the capacitance with the selection of η from 0.01 to 0.99 using the design parameter of the table 3-3, and using different values of r for the sensitivity layer is plotted in Figure 3-12. It is shown that the capacitance of the IDC unit cell decreases smoothly and exponentially with the decreasing metal ratio. In the plot can be seen that the same amount of variation in metal ratio results a more significant change when the initial metal ratio is bigger than 0.9, which means that the interdigital capacitor with a higher metal ratio shows greater sensitivity than the one with a smaller metal ratio. Therefore, in our design of the interdigital capacitor, we tend to set the metal ratio at 0.9. Furthermore, as noticed in the range 0.8-0.9 of η the change of capacitance is nonlinear. Thus, aimed on having a better sensing linearity, we are trying to avoid our design in this range.

Table 3–3: Electrical Parameter Values

DESIGN PARAMETER	VALUE
ε_S	3.9
ε_{poly}	2.25
ε_{PVDF}	10
ε_0	$8.854 \times 10^{-12} F/m$
N	26
L_C	24.1 mm
h1	$35 \mu m$
h2	$110 \mu m$
h3	$100 \mu m$
W_C	$800 \mu m$
G_C	$800 \mu m$

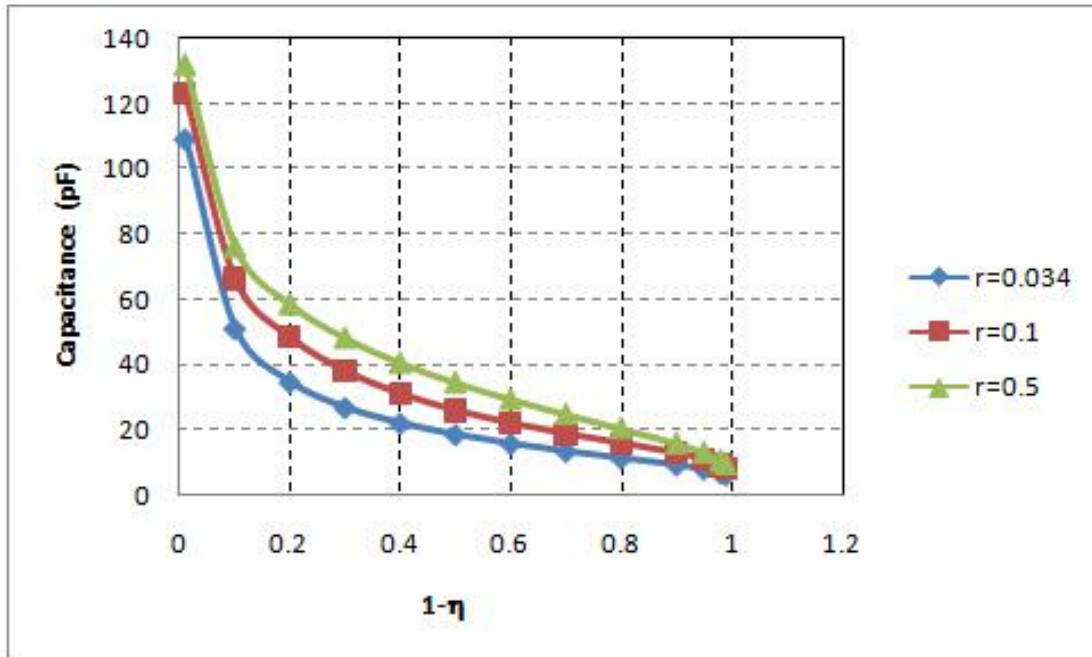


Figure 3–12: Capacitance as a function of η , for a IDC designed with the parameter of the table 3-3

3.2.3 Simulation of the electrostatic field of IDC

This model was done using the MEMS module of COMSOL software and it illustrates how to approach a 3D electrostatics problem, create a geometry using the array and extrusion tools, and compute capacitances using the Electrostatics application modes port boundary condition. The quick 3D analysis of the electrostatic field gives a capacitance value that can be combined with the parallel-plate theory to provide considerable design information. The theoretical background using for the software is:

The energy required to charge a capacitor should equal that of the electrostatic field, which is:

$$W_e = \frac{Q^2}{2C} \quad (3.16)$$

W_e is readily available in the Electrostatics application mode; the software calculates it by integrating across the domain

$$W_e = \iiint_{\Omega} (\mathbf{D} \cdot \mathbf{E}) d\Omega \quad (3.17)$$

where \mathbf{D} is the electric displacement, and \mathbf{E} is the electric field. The capacitance, \mathbf{C} , is related to the charge on the two conductive plates, Q , and the voltage difference across those plates, ΔV , by:

$$C = \frac{Q}{\Delta V} \quad (3.18)$$

Now calculate \mathbf{C} from the stored electric energy in the capacitor, W_e , and the voltage across the capacitor:

$$C = \frac{Q^2}{2W_e} = \frac{C^2 \Delta V^2}{2W_e} \Rightarrow C = \frac{2W_e}{\Delta V^2} \quad (3.19)$$

In the figure 3-13 is shown the design of the IDC using the parameters for the table 3-3 and the design proposed in the figure 3-9

The figure 3-14 shows the mesh of the simulation and the figure 3-15 and 3-16 shows the results

The value of capacitance for the simulation is 19.52 pF, and is shown in the figure 3-17

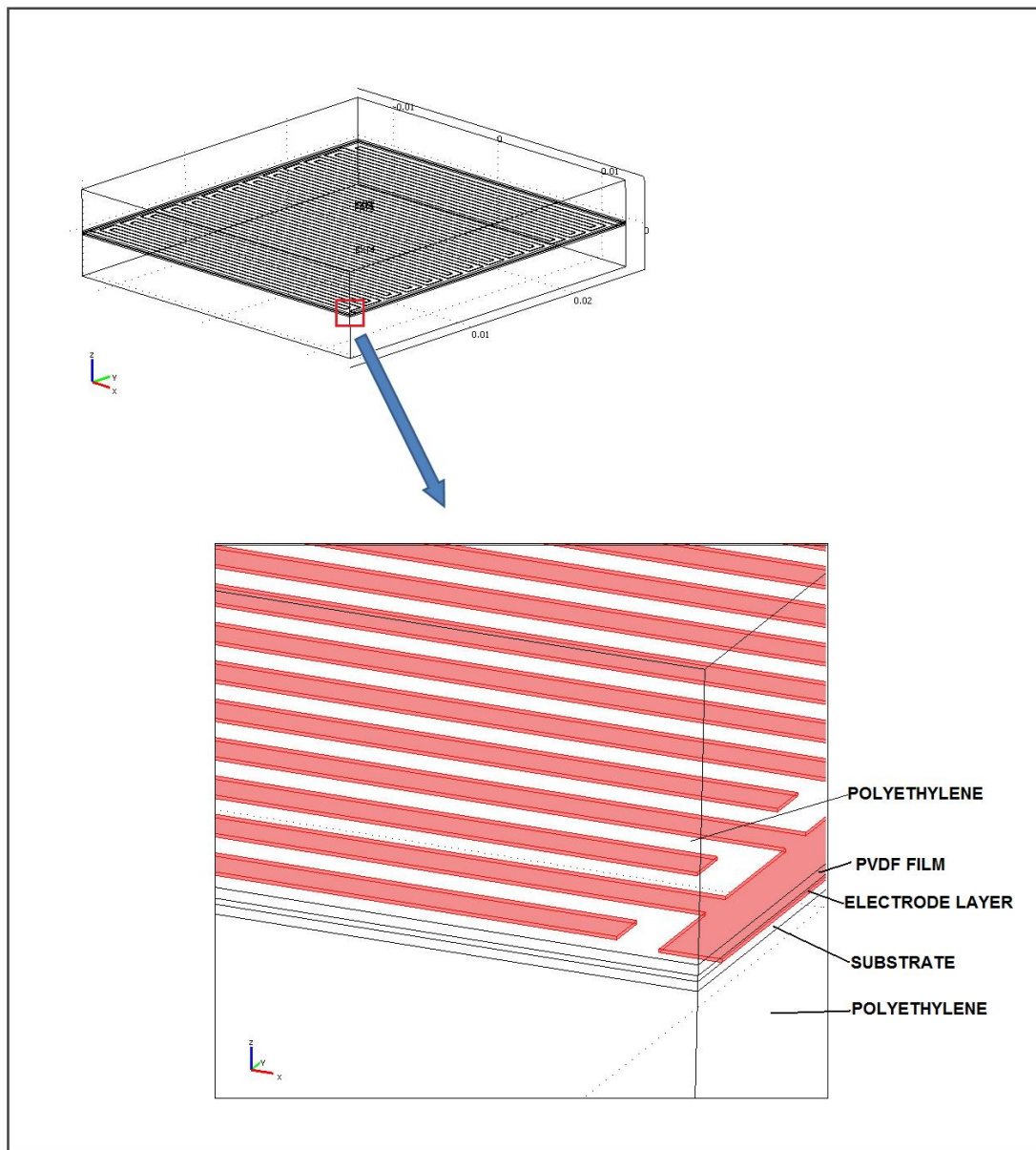


Figure 3-13: Design of the IDC in Comsol

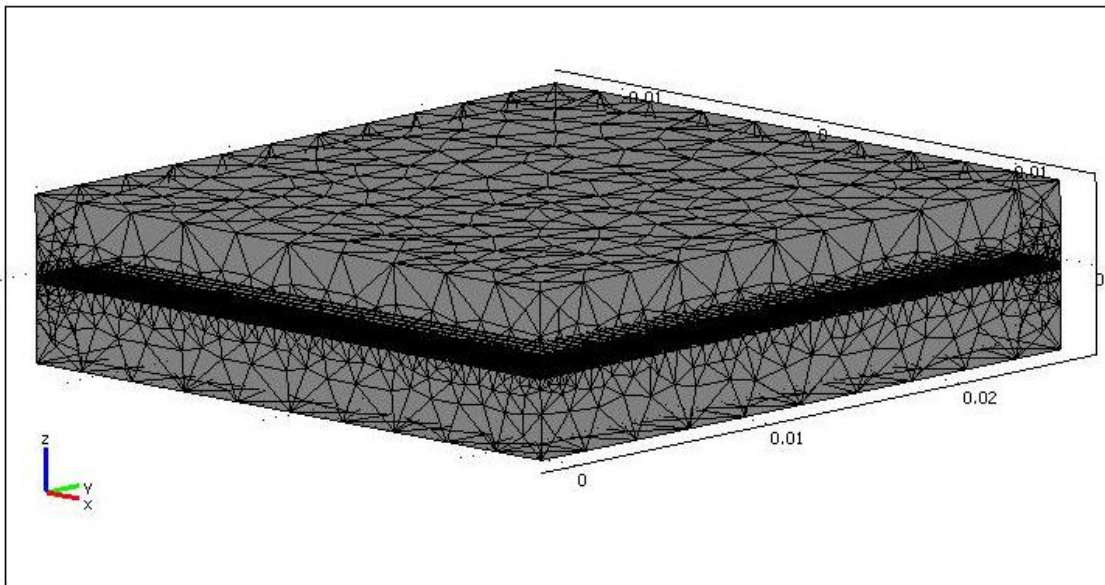


Figure 3-14: Mesh of the simulation

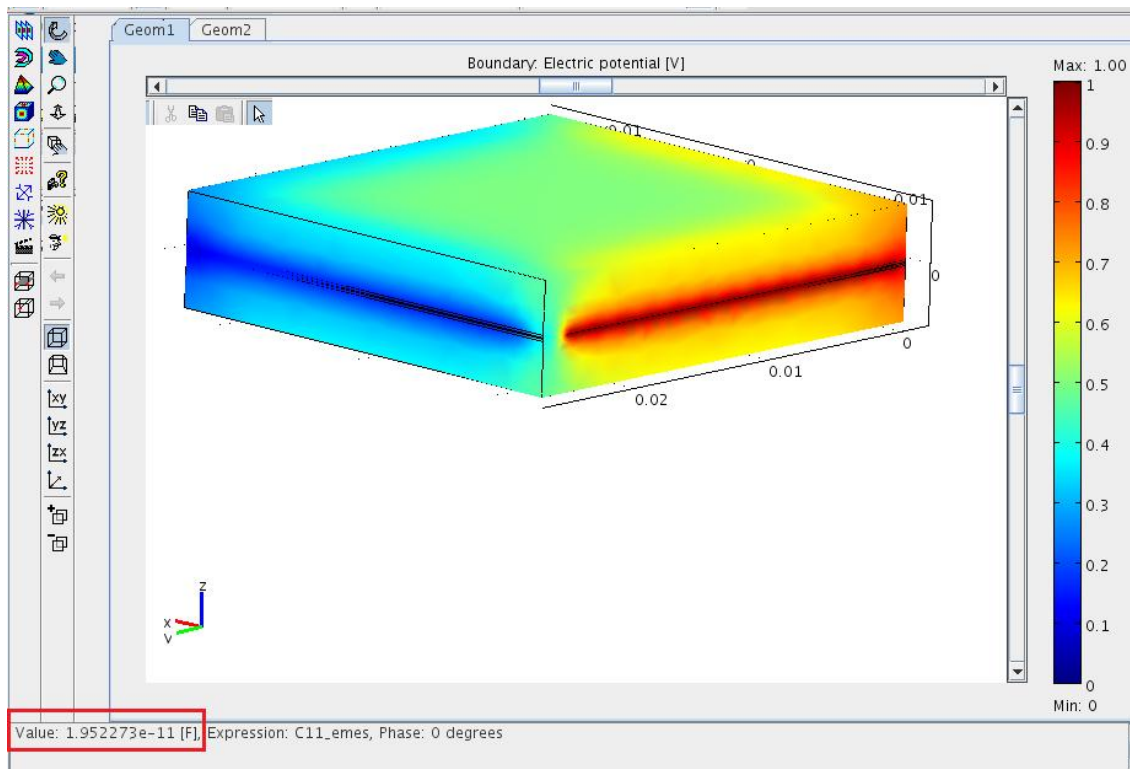


Figure 3-15: Result for the capacitance for the IDC simulation

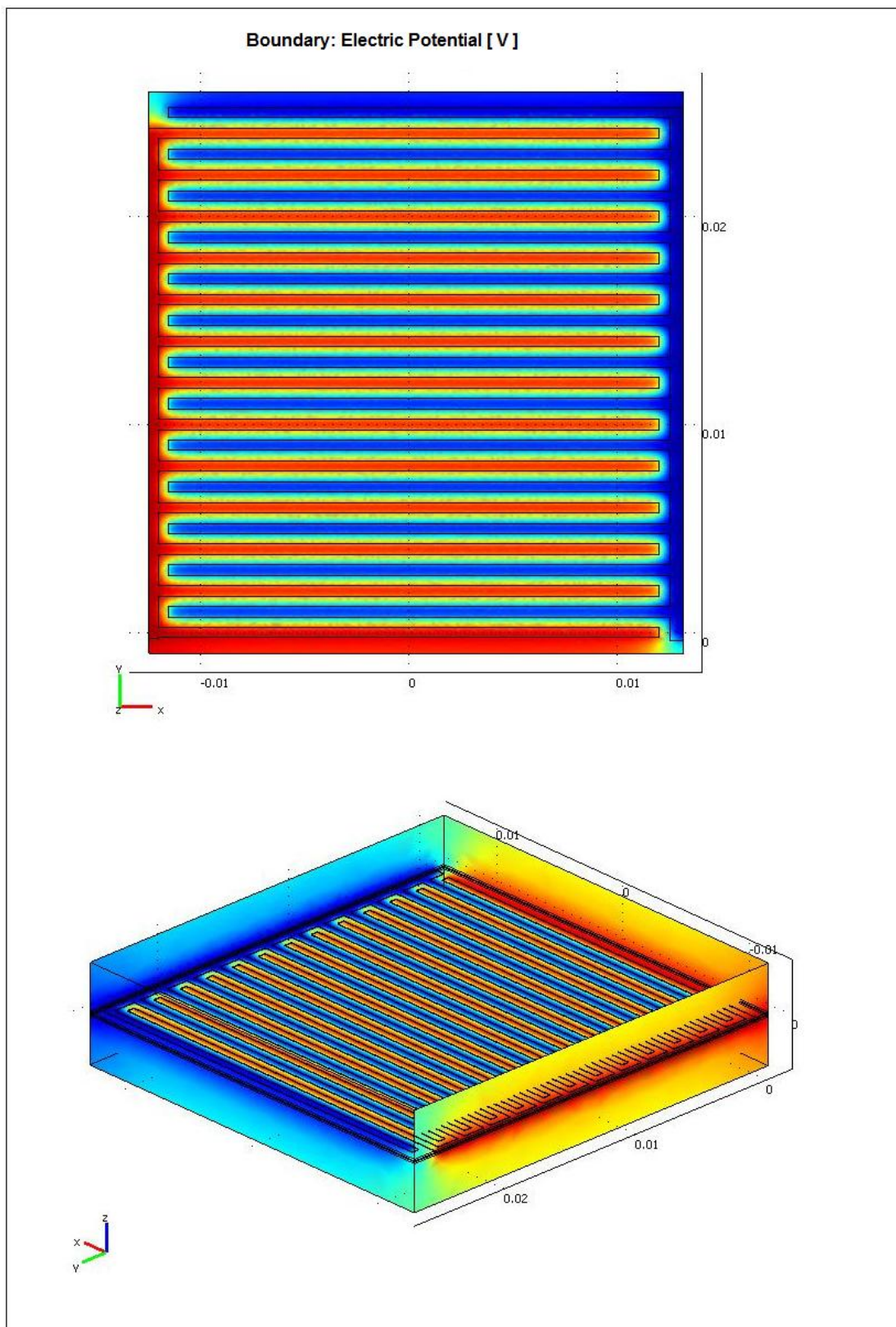


Figure 3-16: Simulation plots results for the electric potential [V]

3.2.4 Pressure Dependent Capacitance

The material of the sensitive layer in the top of the electrodes is Polyvinylidene Fluoride (PVDF) which is a piezoelectric material. The piezoelectric materials have the ability to generate an electric field or electric potential in response to applied mechanical stress. Application of pressure modifies the dielectric constant ϵ_1 of the medium across the electrode structure and correspondingly varies the electric field across it. It is demonstrated that the e-field increases exponentially with applied pressure over a defined pressure range, which makes the system a very sensitive pressure sensor. The pressure applied over the elastomer sheet can change the electric field across the positive and negative electrodes due to the following reasons.

- i) The dielectric permittivity of the sensitive layer changes with applied pressure due to the high compressibility of the medium and hence changes the electric field across the electrodes. In this research the relation between the pressure and the resonant frequency of the sensor will be discussed experimentally.

3.3 Spiral Inductor

The Faraday's Law states that any change in the magnetic environment of a coil of wire will cause a voltage (emf) to be induced in the coil. No matter how the change is produced, the voltage will be generated. The change could be produced by changing the magnetic field strength, moving a magnet toward or away from the coil, moving the coil into or out of the magnetic field, rotating the coil relative to the magnet, etc.

Induction is measured in unit of Henries (H) which reflects this dependence on the rate of change of the magnetic field. One henry is the amount of inductance that is required to generate one volt of induced voltage when the current is changing at the rate of one ampere per second. When induction occurs in an electrical circuit and affects the flow of electricity it is called inductance, L. Self-inductance, or simply inductance, is the property of a circuit whereby a change in current causes a change in voltage in the same circuit. When one circuit induces current flow in a second nearby circuit, it is known as mutual-inductance.

3.3.1 Self- Inductance

Self inductance is defined as the induction of a voltage in a current-carrying wire when the current in the wire itself is changing. In the case of self-inductance, the magnetic field created by a changing current in the circuit itself induces a voltage in the same circuit. Therefore, the voltage is self-induced. The term inductor is used to describe a circuit element possessing the property of inductance and a coil of wire is a very common inductor. In circuit diagrams, a coil or wire is usually used to indicate an inductive component. Taking a closer look at a coil will help understand the reason that a voltage is induced in a wire carrying a changing current. The alternating current running through the coil creates a magnetic field in and around the coil that is increasing and decreasing as the current changes.

The self-inductance of circular loop of round wire has low frequency inductance that can be estimated by [46].

$$L_r \approx n^2 \mu_0 R \left[\ln \left(\frac{8R}{a} \right) - 1.75 \right] \quad (3.20)$$

Where n means the inductor turns, R indicates the loop radius, a corresponds to the wire radius, and the magnetic permeability of free space $\mu_0 = 4\pi \times 10^{-7} \text{ H/m}$.

3.3.2 Mutual Inductance

Mutual inductance occurs when the change in current in one inductor induces a voltage in another nearby inductor. Suppose two coils are placed near each other, as shown in Figure 5-1 [41].

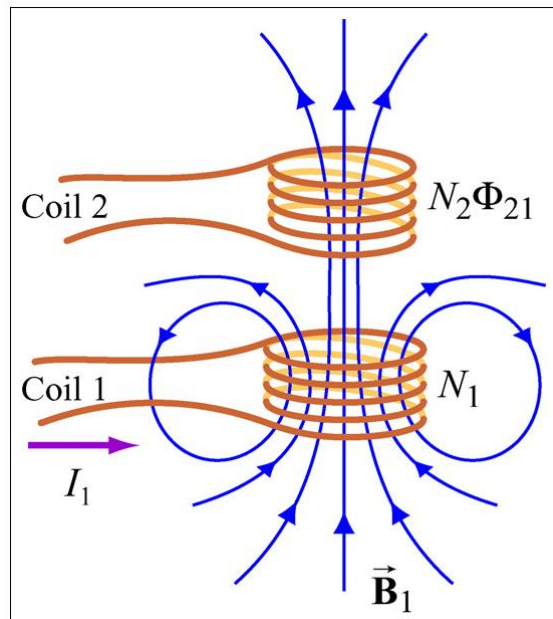


Figure 3–17: Changing current in coil 1 produces changing magnetic flux in coil 2

The first coil carries a current I_1 and has N_1 turns which gives rise to a magnetic field \vec{B}_1 . Due the two coils are close to each other, some of the magnetic field

lines through coil 1 will also pass through coil 2. Let Φ_{21} denote the magnetic flux through one turn of coil 2 due to I_1 [41]. Now, by varying I_1 with time, there will be an induced emf associated with the changing magnetic flux in the second coil:

$$\varepsilon_{21} = -N \frac{d\Phi_{21}}{dt} = -\frac{d}{dt} \iint_{\text{coil } 2} \vec{B}_1 \cdot d\vec{A}_2$$

The time rate of change of magnetic flux Φ_{21} in coil 2 is proportional to the time rate of change of the current in coil 1:

$$N_2 \frac{d\Phi_{21}}{dt} = M_{21} \frac{dI_1}{dt} \quad (3.22)$$

where the proportionality constant M_{21} is called the mutual inductance. It can also be written as

$$M_{21} = \frac{N_2 \Phi_{21}}{I_1} \quad (3.23)$$

The SI unit for inductance is the henry (H)

The mutual inductance also has a relationship with the coupling coefficient. The coupling coefficient is always between 1 and 0, and is a convenient way to specify the relationship between a certain orientation of inductor with arbitrary inductance:

$$M = k \sqrt{L_1 L_2} \quad (3.24)$$

where k is the coupling coefficient ($0 \leq k \leq 1$), L_1 is the inductance of the first coil, and L_2 is the inductance of the second coil.

4 PERFORMANCE ANALYSIS

Sensor performance analysis will be investigated in this Chapter in order to obtain an optimal sensor configuration with high Q-factor, high sensitivity, small size and long communication distance.

4.1 Modeling and Simulation

The remote reader across inductive powering will generate a magnetic field induced by an alternating current and the proposed pressure sensors will be placed within that magnetic field as shown in Figure 4-1. In this resonant circuit Z_R and Z_S indicates the inherent impedances from the reader and sensor respectively, R_R and R_S are the self resistances from the reader and sensor, C_R is the capacitance of the reader, which is introduced in order to maximize the current applied through the reader antenna, C_S is the sensor capacitance, which is sensitive to environment pressure, L_R and L_S indicates the inductance from reader and sensor respectively. Z'_s is the reflected impedance of the sensor, Z_i is the input impedance seen from the reader side, and M corresponds to the mutual inductance[54].

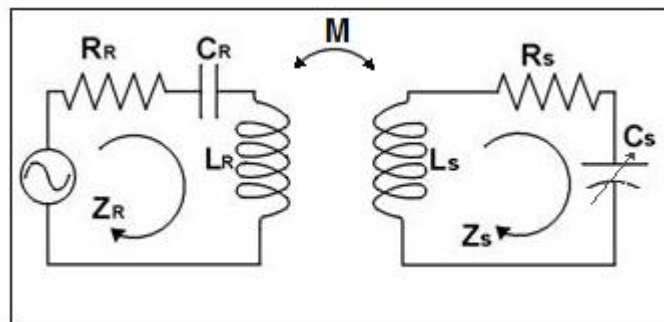


Figure 4-1: Inductive Coupled Reader and LC Sensor

Eliminate the coupled reader coil and the sensor by reflecting impedances back to the reader is an approach to analyze this resonant circuit, this method is used in order to clarify the voltage change of reader coil. The equivalent circuit diagram of the resonant circuit of the reader with the inductive coupled sensor is shown in Figure 5-2.

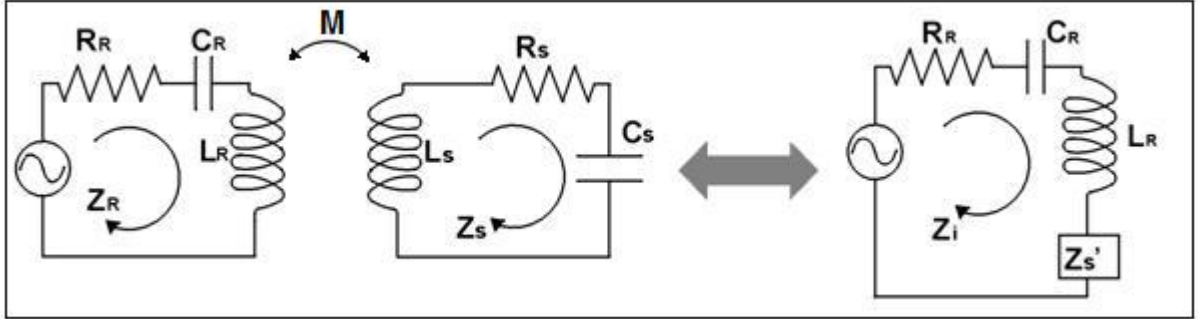


Figure 4-2: Equivalent Circuit Diagram of Wireless Telemetry System

The impedance of the resonant circuit of the reader is given by:

$$Z_R = j\omega L_R + R_R + \frac{1}{j\omega C_R} \quad (4.1)$$

The impedance of the sensor side can be expressed as:

$$Z'_S = \frac{(\omega M)^2}{j\omega L_S + R_S + \frac{1}{j\omega C_S}} = -\frac{\omega^2 k^2 L_R L_S}{j\omega L_S + R_S + \frac{1}{j\omega C_S}} \quad (4.2)$$

where k is the coupling factor, defined by:

$$k = \frac{M}{\sqrt{L_R L_S}} \quad (4.3)$$

The sensor interaction can be seen as a load variation $\Delta Z'_S$ placed in series with the inductance antenna, defined by:

$$\Delta Z'_S = \frac{\omega^2 k^2 L_R L_S}{j\omega L_S + R_S + \frac{1}{j\omega(C_S + \Delta C_S)}} \quad (4.4)$$

The input impedance seen from the reader side is defined by:

$$Z_i = Z_R + Z'_S \quad (4.5)$$

Using the equation 5.1 and 5.2 into 5.5, we have the input impedance seen from the reader defined by:

$$Z_i = j\omega L_R + R_R + \frac{1}{j\omega C_R} + \frac{w^2 k^2 L_R L_S}{j\omega L_S + R_S + \frac{1}{j\omega(C_S + \Delta C_S)}} \quad (4.6)$$

The reflected impedance Z'_S multiplied by the current is equivalent to the voltage drop caused by the sensor side circuit.

In the portable reader a signal is used to generate a periodical sweep of the frequency around the sensors resonant frequency to measure a frequency variation. A sudden increase in the sensor impedance Z'_S occurs, when the excitation frequency coincide the sensor's resonant frequency. The figures 5-3 to 5-7 shows the magnitude of impedance of the sensor impedance Z'_S in response to the sweeping changes, the parameter values in table 5.1 where used for the figure.

When pressure increases or decrease, induces the variation of sensors capacitance C_S , and thus the input impedance Z_i . It can be seen that when the pressure increases, the resonant frequency will decrease and the peak of the input impedance Z_i will move toward to the left accordingly the curve shown in Figure 4-3 to 4-7 was simulated using the same parameter values shown in Table 4.1.

Table 4-1: Electrical Parameter Values

PARAMETER	SYMBOL	POLYURETHANE	PDMS
Sensor Nominal Capacitance	C_s	29.3 pF	17.9 pF
Sensor Inductance	L_s	5.57 μ H	5.57 μ H
Resonant Frequency	f_o	12.44Mhz	15.91Mhz
Sensor Resistance	R_s	0.5 Ω	0.5 Ω
Reader Inductance	L_r	0.1169 μ H	0.1169 μ H
Reader Radius	r_R	2.25cm	2.25cm
Inductor Radius	r_S	2cm	2 cm
Coupling Distance	d	1 cm	1 cm
Nominal Coupling Factor k	k	0.6395	0.6395

Table 4-2: Electrical Parameter Values for Interdigital sensor

PARAMETER	SYMBOL	PDMS
Sensor Nominal Capacitance	C_s	19.4 pF
Sensor Inductance	L_s	5.57 μ H
Resonant Frequency	f_o	17.44Mhz
Sensor Resistance	R_s	0.5 Ω
Reader Inductance	L_r	0.1169 μ H
Reader Radius	r_R	2.5cm
Inductor Radius	r_S	2cm
Coupling Distance	d	1 cm
Nominal Coupling Factor k	k	0.6395

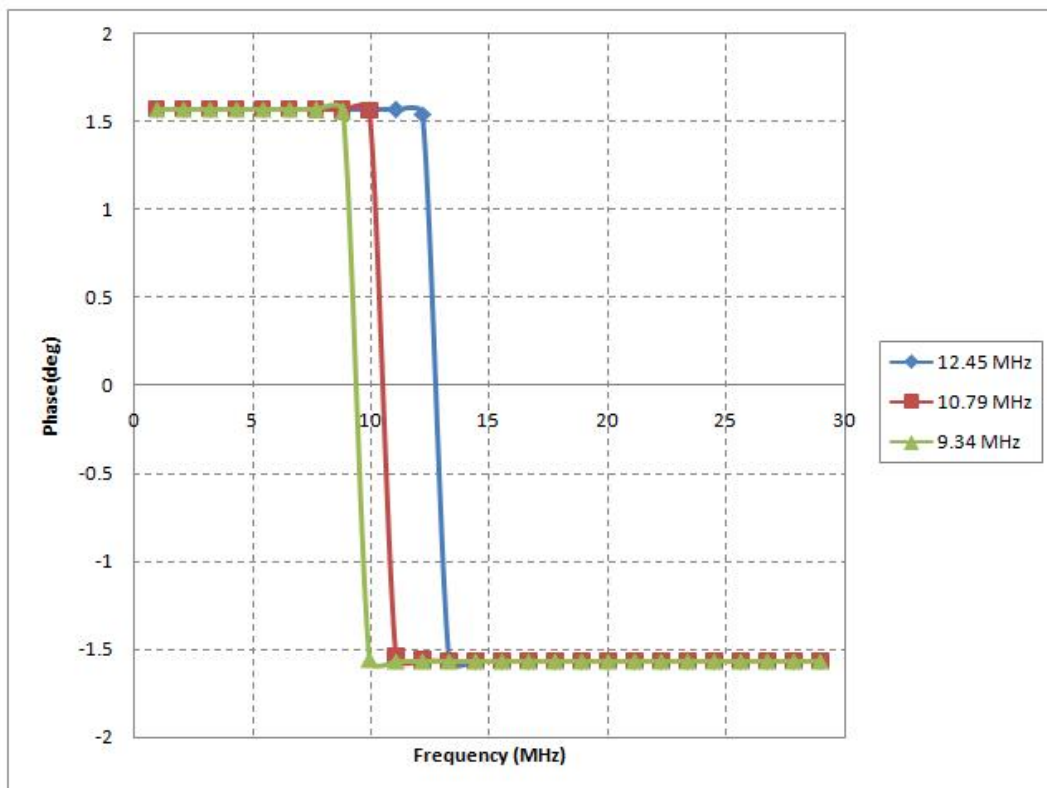
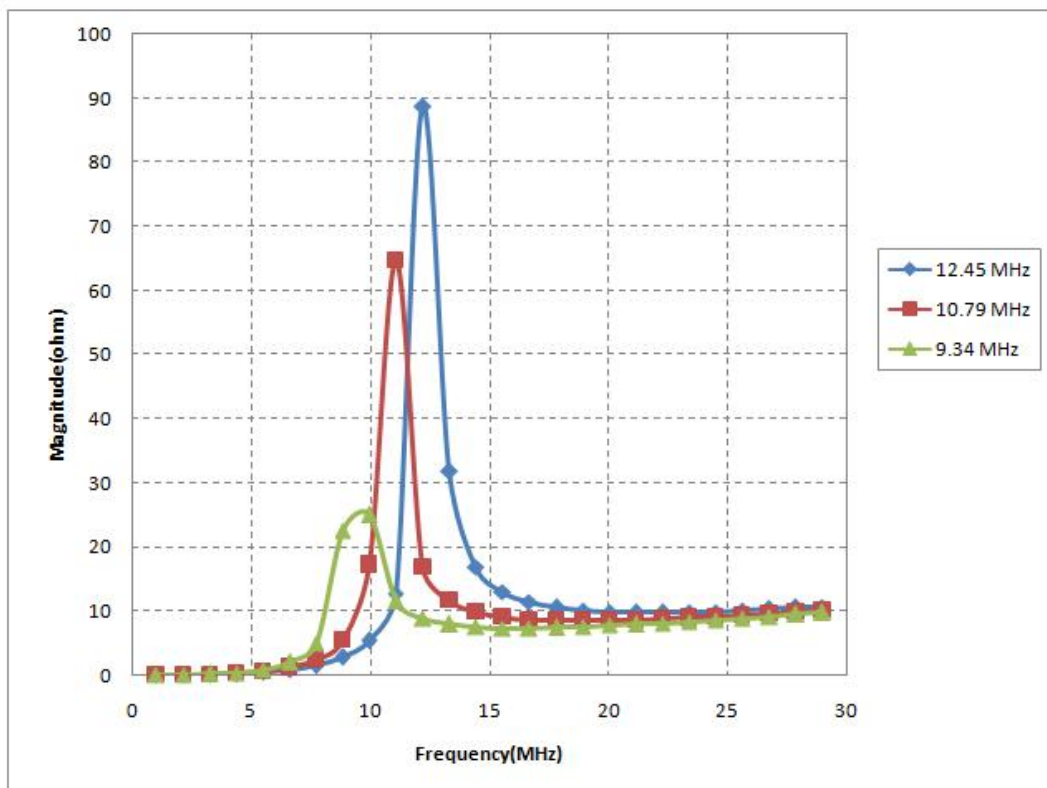


Figure 4-3: Magnitude and Phase Angle of Zs Polyurethane

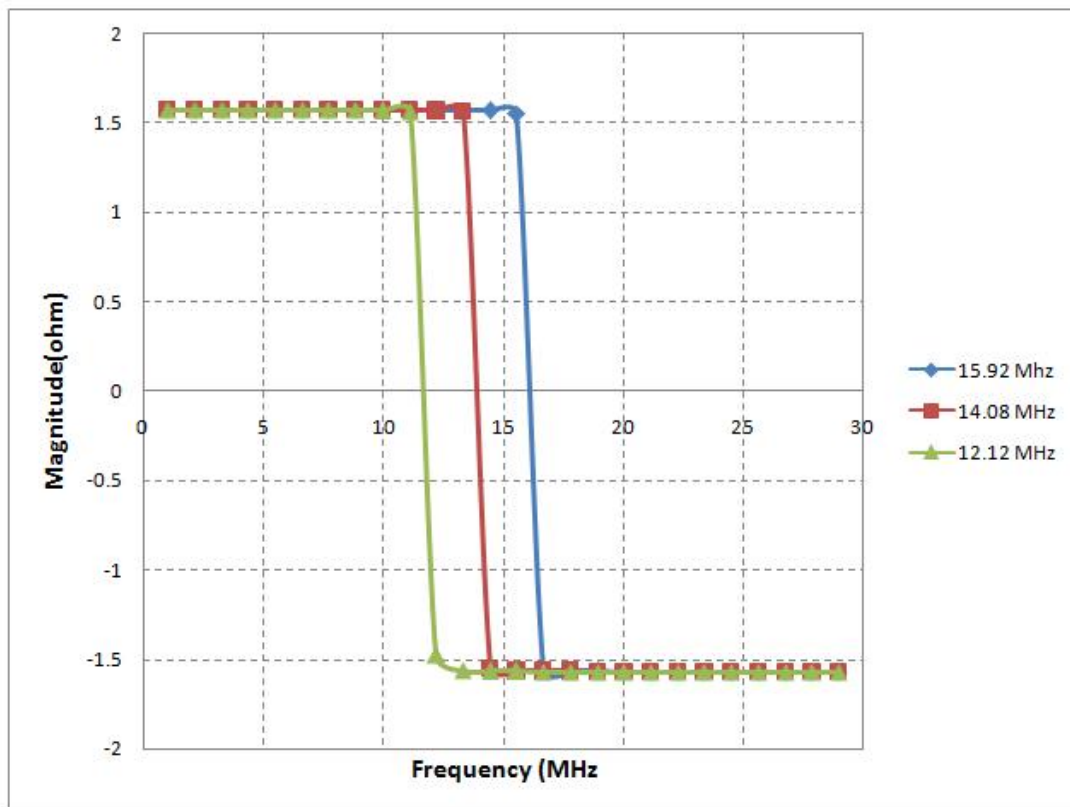
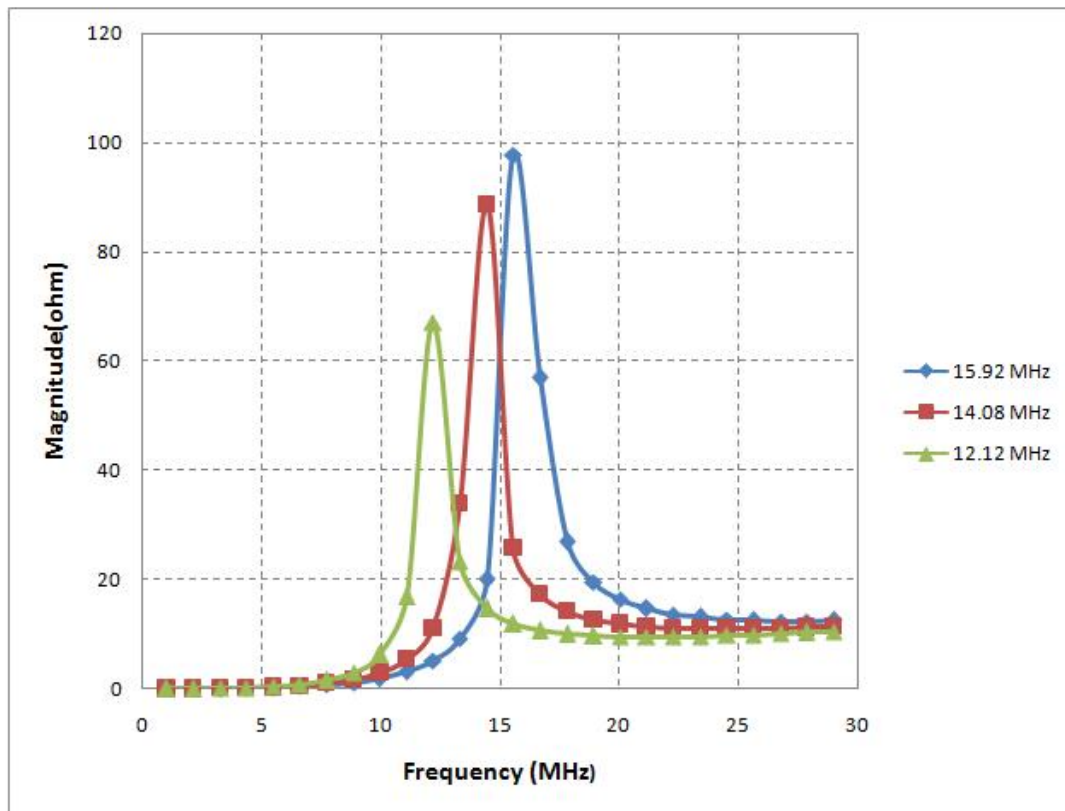


Figure 4-4: Magnitude and Phase Angle of Zs PDMS Parallel Plate

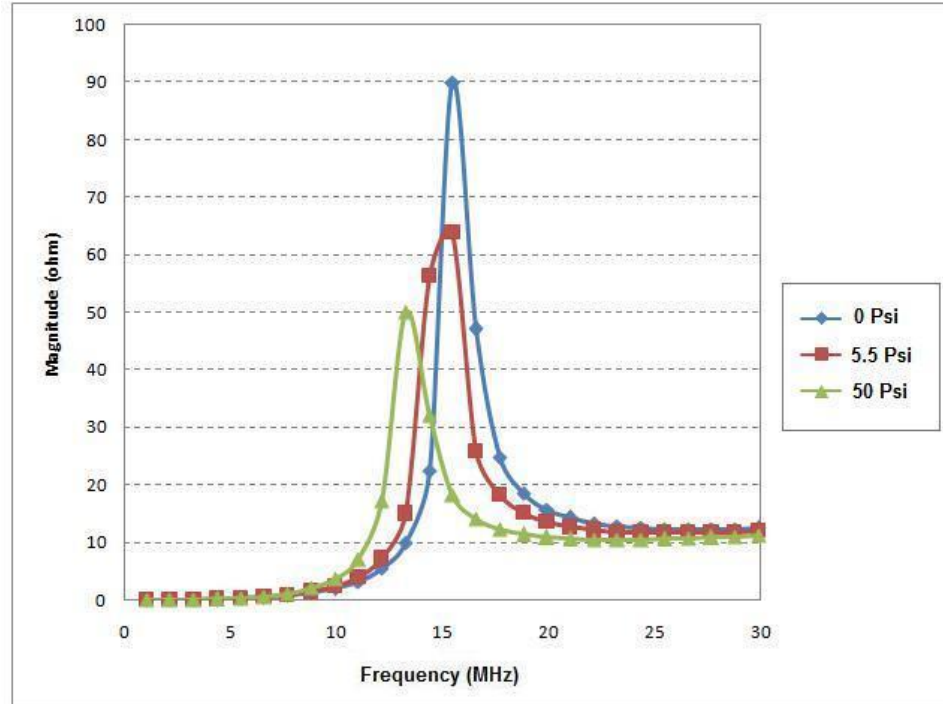


Figure 4-5: Resonant Frequency of Input Impedance vs. Pressure IDC PVDF

4.2 Performance Analysis

The reflected impedance Z'_S must be high enough in order to detect the resonant frequency from the reader's side, for that reason, the coupling coefficient and Q-Factor should be high enough to make sure the resonant frequency lecture. In this section the sensor performance will be analyzed which includes the resonant frequency, Q-Factor and Coupling Distance.

4.2.1 Resonant Frequency

A condition of resonance will be experienced in a LC circuit when the reactances of the capacitor and inductor are equal to each other. Because inductive reactance increases with increasing frequency and capacitive reactance decreases with increasing frequency, there will only be one frequency where these two reactances will be

equal. The equations for determining the reactance of a capacitor and an inductor respectively are:

$$X_C = \frac{1}{2\pi f\mathbf{C}} \quad (4.7)$$

$$X_L = 2\pi f\mathbf{L} \quad (4.8)$$

If we want to find the point where the two reactances are equal to each other, we can set the two reactance equations equal to each other and solve for frequency algebraically:

$$X_L = X_C = 2\pi f\mathbf{L} = \frac{1}{2\pi f\mathbf{C}} \quad (4.9)$$

Eliminating the f term in the denominator of the fraction, we have:

$$2\pi f^2\mathbf{L} = \frac{1}{2\pi\mathbf{C}} \quad (4.10)$$

Leaving f^2 by itself on the left-hand side of the equation, we have:

$$f^2 = \frac{1}{2\pi 2\pi\mathbf{LC}} \quad (4.11)$$

Taking the square root of both sides of the equation leaves f itself on the left side, we have

$$f = \frac{\sqrt{1}}{\sqrt{2\pi 2\pi\mathbf{LC}}} \quad (4.12)$$

Simplifying :

$$f = \frac{1}{2\pi\sqrt{\mathbf{LC}}} \quad (4.13)$$

So there we have it: a formula to tell us the resonant frequency of a tank circuit, given the values of inductance (L) in Henrys and capacitance (C) in Farads.

What happens at frequency resonance is quite interesting. With capacitive and inductive reactances equal to each other but with opposite signs, the total impedance increases to infinity, meaning that the tank circuit draws no current from the AC power source. If we use the parallel impedance formula to see what happens to total Z,

$$Z_{parallel} = \frac{1}{\frac{1}{Z_L} + \frac{1}{Z_C}} \quad (4.14)$$

$$Z_{parallel} = \frac{1}{\frac{1}{|Z_L|\angle 90^\circ} + \frac{1}{|Z_C|\angle -90^\circ}} \quad (4.15)$$

$$Z_{parallel} = \frac{1}{0} \quad (4.16)$$

Because one may not divided any number by zero and arrive at a meaningful result, but we can say that the result approaches a value of infinity as the two parallel impedances get closer to each other. What this means in practical terms is that, the total impedance of a LC circuit is infinite at resonance frequency.

4.2.2 Q-factor

The quality of a LC resonant circuit is the Q, quality factor. A higher value for this factor means a more narrow bandwidth, which is desirable in many applications. In general, the Q factor is the ration of power stored to power dissipated in the circuit reactance and resistance:

$$Q = \frac{P_{stored}}{P_{dissipated}} \quad (4.17)$$

Also the Q factor, can be defined as the ratio of total stored energy to dissipated energy per unit cycle in this equation:

$$Q = \frac{W_{total}}{P/2\pi f} = \frac{2\pi f W_{total}}{P} \quad (4.18)$$

Where P means the average dissipated power, W is the total stored energy and f is the resonant frequency.

At the resonant frequency, the parallel LC circuit is resistive. At resonance $X_L = X_C$, the reactive components cancel and the impedance is maximum at resonance. Below the resonant frequency, the series resonant circuit looks inductive since the impedance of the inductor is lower, drawing the larger proportion of current. Above resonance, the capacitive reactance decreases, drawing the larger current, thus, taking on a capacitive characteristic. Impedance is maximum at resonance in a parallel resonant circuit, but decreases above or below resonance. Voltage is at a peak at resonance since voltage is proportional to impedance ($E = IZ$). A low Q due to a high resistance in series with the inductor produces a low peak on a broad response curve for a parallel resonant circuit. Conversely, a high Q is due to a low resistance in series with the inductor. This produces a higher peak in the narrower response curve, the simplified expression of Qfactor is defined by:

$$Q = \frac{2\pi f l_S}{R_L} = \frac{1}{R_L} \sqrt{\frac{L_S}{C_S}} \quad (4.19)$$

Here, R_L is the total sensor resistance consisting of the inductor resistance, capacitor resistance and circuit resistance [55].

4.2.3 Coupling Factor

The grade of coupling of two coils is expressed by the coupling factor k, and this factor can be explained as how are the coils coupled. If we have two coils at a certain

distant, and works as the receiver coil and the other one is the transmitter coil, only a fraction of the magnetic flux generated by the transmitter coil, is received by the receiver coil and contributes to the power transmission. The better the coils are coupled, the more flux reaches the receiver. The coupling factor is determined by the distance between the inductors and their relative size. It is further determined by the shape of the coils and the angle between them. If coils are axially aligned, a displacement causes a decrease of k . A fair approximation of k related to design parameter is given by [27] :

$$k = \left(\frac{r_s r_R}{d^2 + r_R^2} \right)^{1.5} \quad (4.20)$$

Where r_R corresponds to the radius of primary coil, r_s indicates the radius of the sensor inductor, and d means the coupling distance.

The self-inductance of circular loop of round wire has low frequency inductance that can be estimated by [46].

$$L_r \approx n^2 \mu_0 R \left[\ln \left(\frac{8R}{a} \right) - 1.75 \right] \quad (4.21)$$

Where n means the inductor turns, R indicates the loop radius, a corresponds to the wire radius, and the magnetic permeability of free space $\mu_0 = 4\pi \times 10^{-7} H/m$. For a reader made of a circular loop with a radius $R = 0.075m$, turns $n = 8$ and a wire radius $a = 1mm$, the self inductance is $28\mu H$.

4.3 Conclusions

In this chapter was investigated the performance analysis of the proposed sensors with respect to resonant frequency, Q-factor and coupling factor. And was concluded that changing parameters such as: the sensor inductance, the radius ratio of the sensor inductor and reader coil, the sensor resistance, the radius of the

reader antenna, the reader inductance; in a optimal way we can have a high performance of the proposed sensors, with high Q-factor, high sensitivity, small size and long communication distance.

5

SENSOR FABRICATION AND EXPERIMENTAL RESULTS

Sensor prototypes fabrication and experimental results are discussed in this chapter. For the parallel plates capacitor prototypes is explained the fabrication process and the Microelectromechanical system (MEMS) technique is briefly explained for the fabrication of the interdigital capacitor

5.1 Fabrication Parallel Plates Pressure Sensor

For MEMS systems the Polydimethylsiloxane (PDMS) is the elastomer most commonly used. Due PDMS offers good chemical and thermal stability this material is widely used for molding microfluidic channels and reactors. Polyurethanes can offer a wide degree of elasticity (with stiffnesses covering an adjustable range depending on chemical formula) as well as excellent chemical resistance to common processing chemicals [56]. Micro molding techniques developed for PDMS can be applied to polyurethanes as well. A commonly used PDMS elastomer (Sylgard-184) was used in this research and a polyurethane RTV liquid rubber. The fabrication process for each prototype using the polyurethane RTV liquid rubber and PDMS is the same, the difference is that the Sylgard-184 PDMS is cured with 10:1 resin to curing agent (from the manufacturer) and the polyurethane RTV liquid rubber consists in two parts: (Poly 74-20, part A: polyurethane pre-polymer and part B: polyol, PolytekDevelopment Co., PA, USA) which is vulcanized to very soft and robust rubber, is used to form the intermediate polymer layer. The softness of the rubber can be adjusted by changing the proportion of the parts. Later of several

combinations of parts in order to get the right softness was found that the formulation of part A:B=1:1 shows good performance with the softness. The mix solution of rubber was applied to the upper surface of the plate base or bottom plate and the top plate was place on it. In the figure 5-1 is detailed the fabrication process and the figure 5-2 and 5-3 is shown a picture of the prototype.

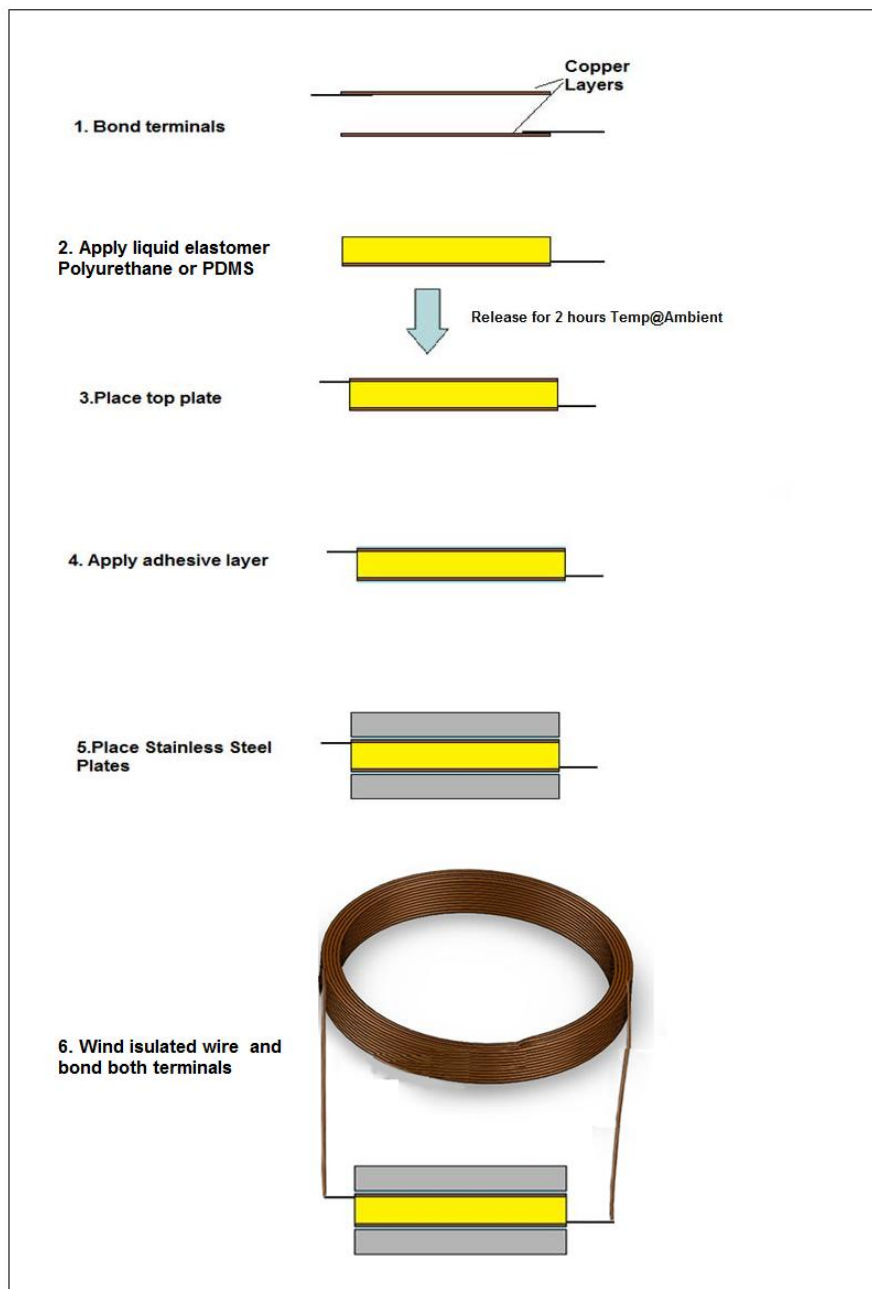


Figure 5–1: Detailed Fabrication Process for parallel plate pressure sensor

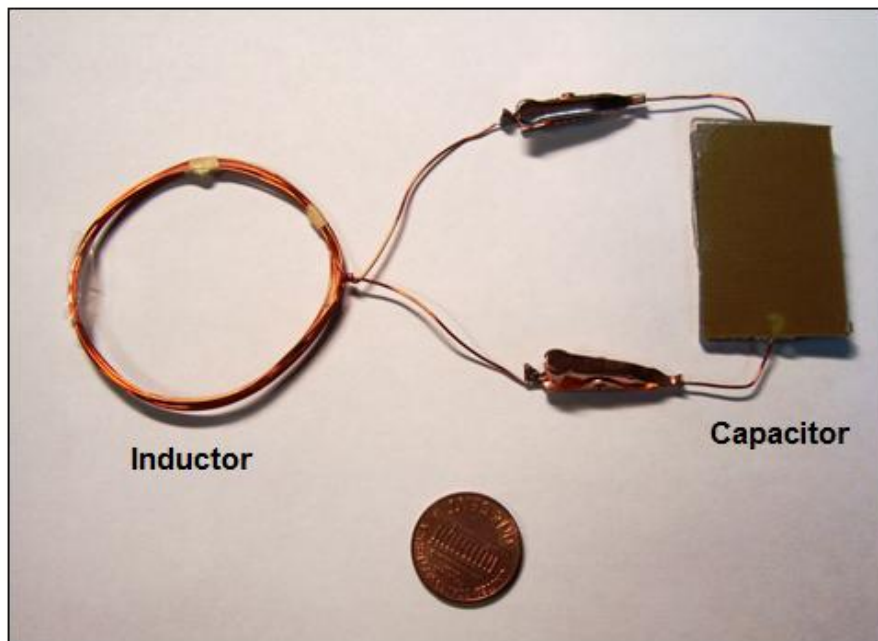


Figure 5-2: Sensor Prototype of parallel plate pressure sensor

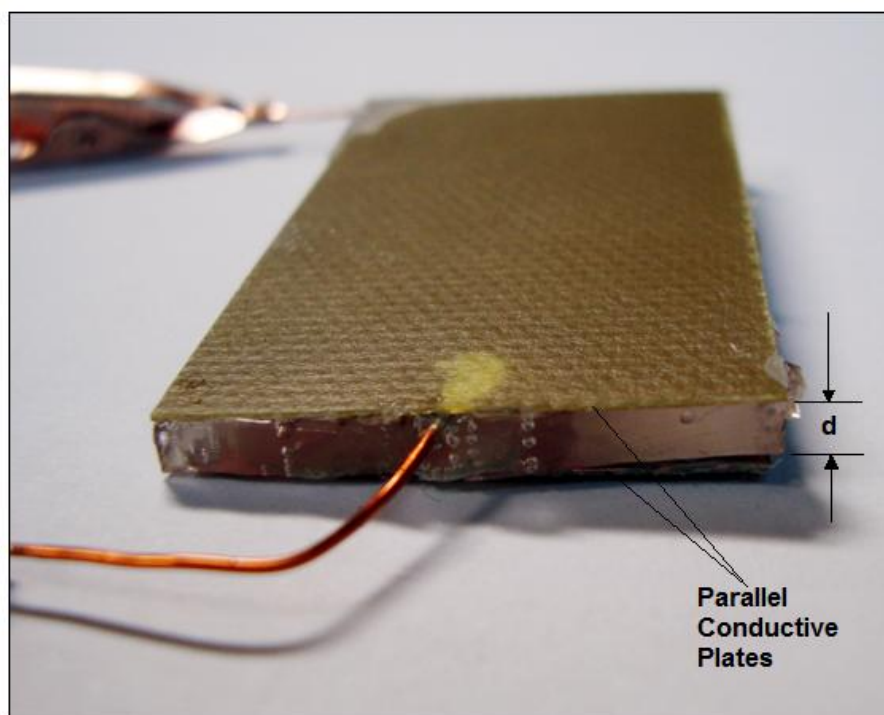


Figure 5-3: Lateral view of Prototype for PDMS material

5.2 Fabrication Interdigital Pressure Sensor

In this chapter we will discuss sensor fabrication using fabricating microelectromechanical system (MEMS) technique. MEMs are a collection of sensor and actuators that can sense its environment and have ability to react in that environment using a microcircuit control. Micromachining is the fundamental technology for the fabrication of MEMS devices. For the fabrication of the interdigital pressure sensor we will use the photolithography process which is one of the most important approach in bulk micromachining. Photolithography is a process used in microfabrication to selectively remove parts of a thin film. It uses light to transfer a geometric pattern from a photomask to a light-sensitive chemical (photoresist) on the substrate. A series of chemical treatments then engraves the exposure pattern into the material underneath the photoresist.

For this work we will use the following materials: The pattern-transfer target material for the main circuit of the sensor is Dupont Pyralux AC single copper-cald laminate which is all-polymide composite of polymide film on copper foil. Polymide base substrate thickness are available from $25\mu m$ to $45\mu m$, Rolled-annealed (RA) copper foil thickness from $18\mu m$ to $35\mu m$, and electro-deposited (ED) copper foil tickness from $25\mu m$ to $45\mu m$. The basic procedure for Photolithography is briefly explaind :

1. Cleaning. The laminated copper clad is cleaned with a solvent to remove the contaminants on the surface. Clean surface condition would offer a better contact for the applied photoresist and provide a good cicuit condition.
2. Preparation. Apply a thin layer of photoresist on the surface of the copper clad and make it spread all over the surface instead of just dropped on one point on the surface. In order to get a uniform thin layer is used a spin coating which typically runs at 1200 to 4800 rpm for 30 to 60 seconds.

3. Exposure. A transparent photographic film which contains the pattern of the desired circuit is aligned on the soft baked copper clad. Make sure that the ink side on the pattern film is the side that attached to the photoresist. Turn on the UV light and start the timer for 90 seconds.
4. Developing. Remove the mask pattern film and replace the copper clad into the developer solvent which is 1:1 solution of AZ developer and deionized water. Hold the clad with tweezers and agitate mildly until the photoresist which is exposed to the UV light has been fully dissolved left a legible patterned part on the copper which is the same as the mask pattern.
5. Etching. Leave the copper clad into the hard baking oven at 120 C for 60 minutes. Cool it and immerse it into the solutions of a board etchant. Hold the clad with tweezers and agitate mildly until the copper which is not covered by the hard-baked photoresist is completely etch away.

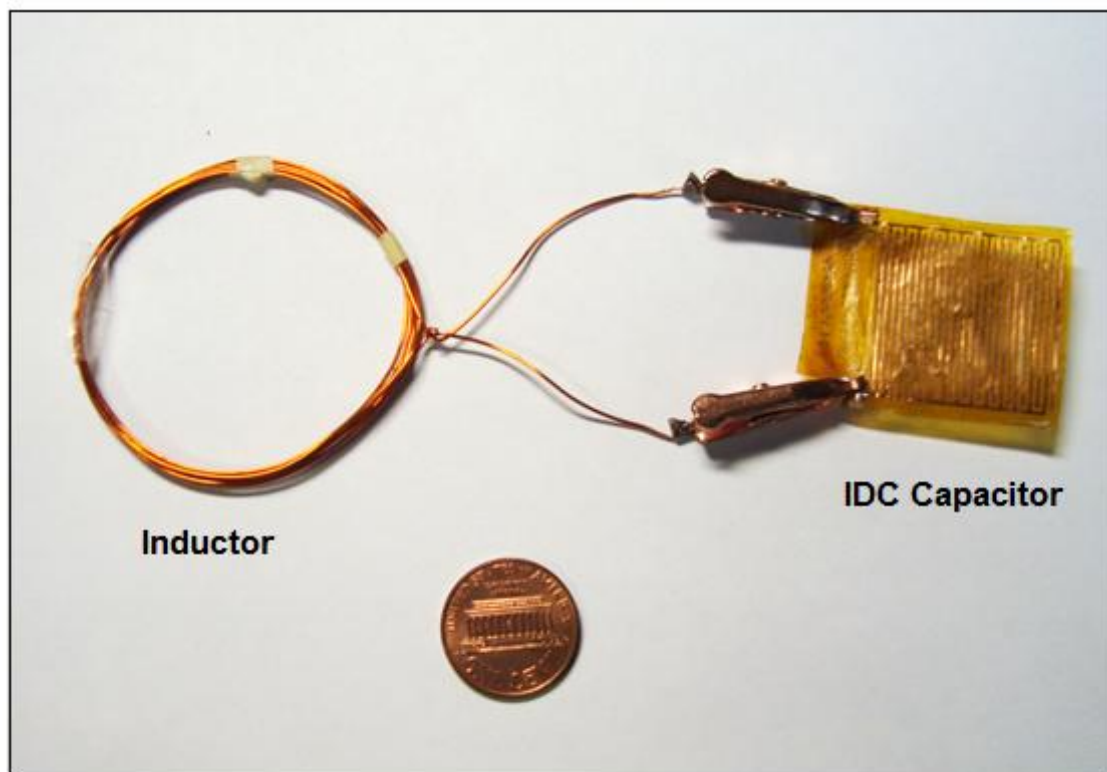


Figure 5-4: Sensor Prototype of IDC pressure sensor

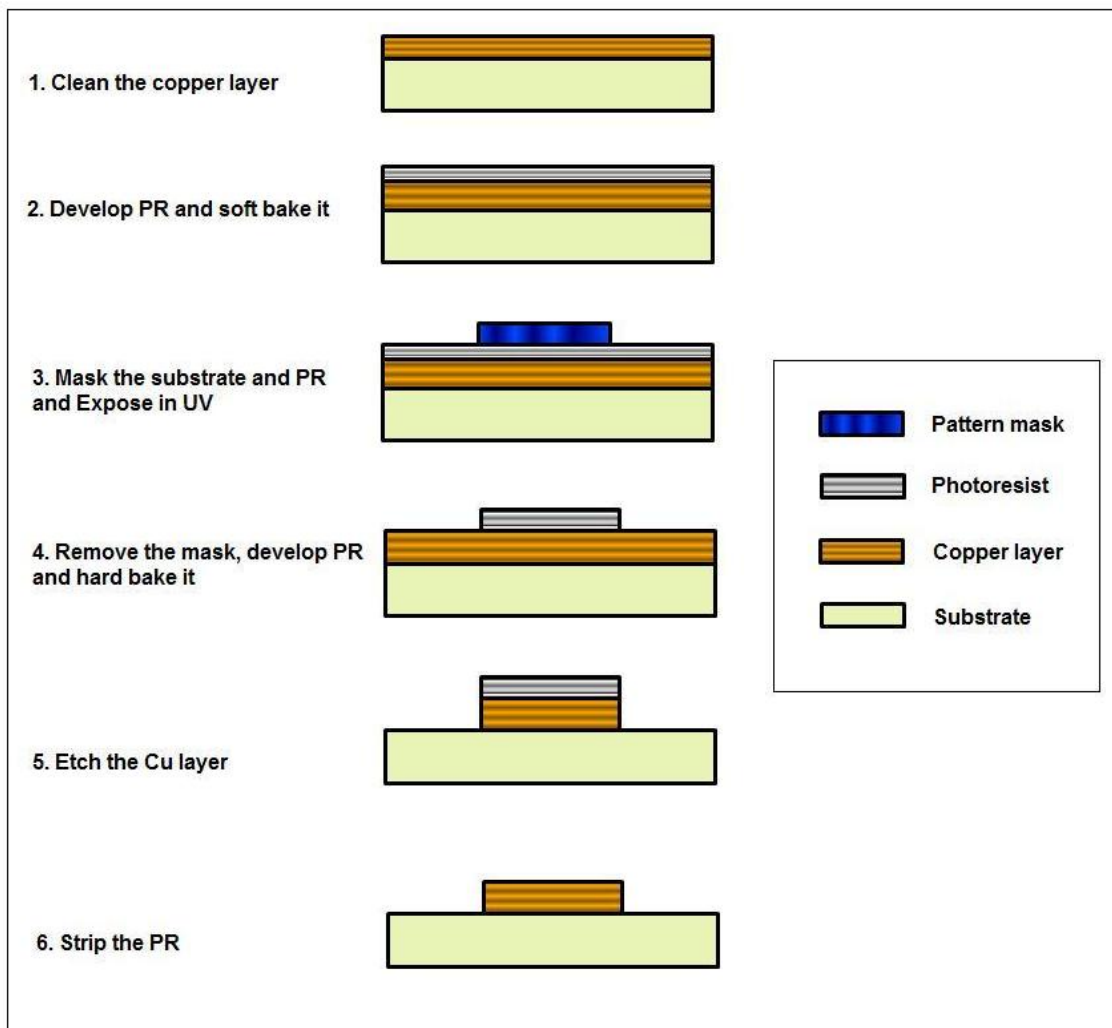


Figure 5-5: Illustration on the sensor fabrication using photolithography.

5.3 Experimental Results

The test and calibration for the proposed sensors was developed using a machine to measure compression forces. This machine consists in a lead worm and a gear, with the machine's crank is developed an input movement and an output movement generates a compression force to sample we want to applied the force. This compression force is detected and measure by the load cell and converted to voltage signal, this signal is send out to an external device and converted to force units by software and a data acquisition device. In the figure 5-6 is shown a schematic view of the testing machine.

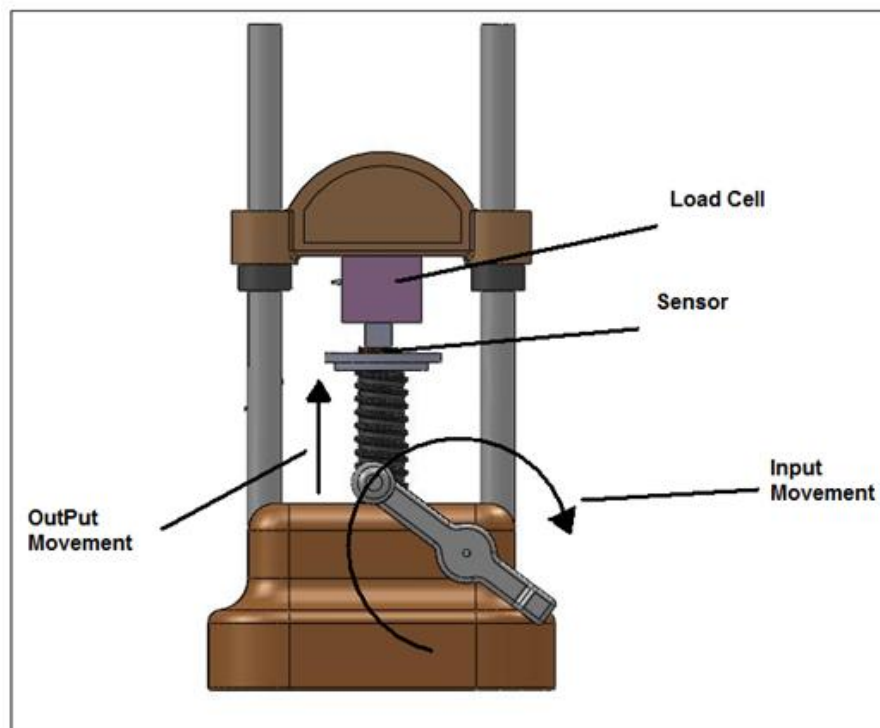


Figure 5-6: Schematic view of the compression testing machine

A compression force is applied to the sensor using the compression machine and the value of this force is shown by the load cell data acquisition device; at the same time, the antenna of the reader was laid near to the inductor coil of the proposed sensors which transferred the pressure information to the reader. This information can be read out from the laptop in terms of impedance response or the reader.

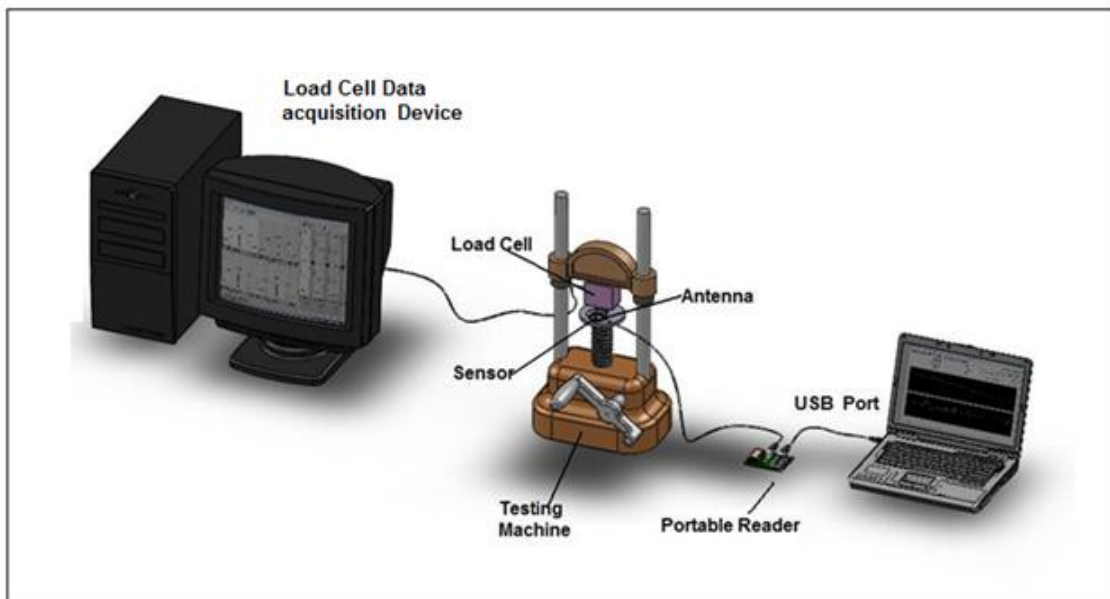


Figure 5-7: Principle of Sensor Calibration Experiment

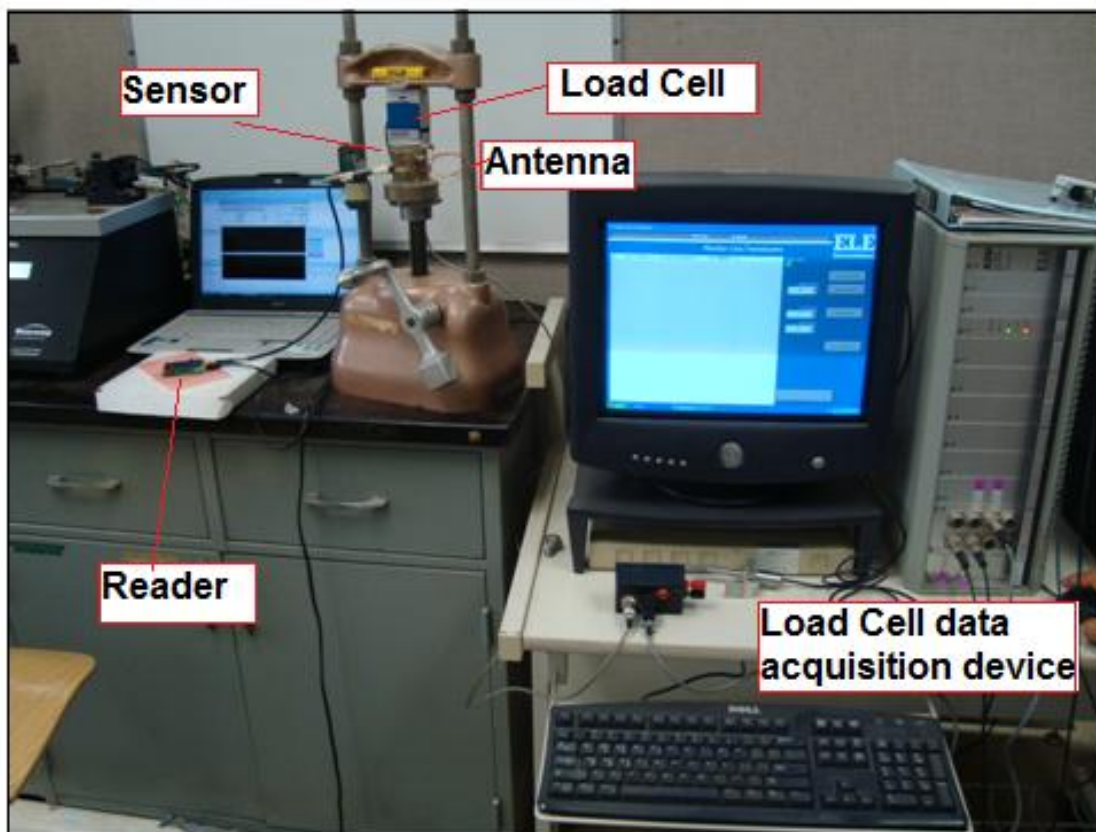


Figure 5-8: Calibration test setup up

5.3.1 Parallel Plate

For the parallel plate pressure sensor proposed were done two experiment for each material (Polyurethane and PDMS). In the figures 5-9 and 5-10 are shown the experimental relationship between the pressure applied and the Resonant frequency of the sensor using PDMS and polyurethane respectively. The figures 5-11 and 5-12 show the relation of the resonant frequency and the experimental impedance response of the prototypes when is applied different pressure.

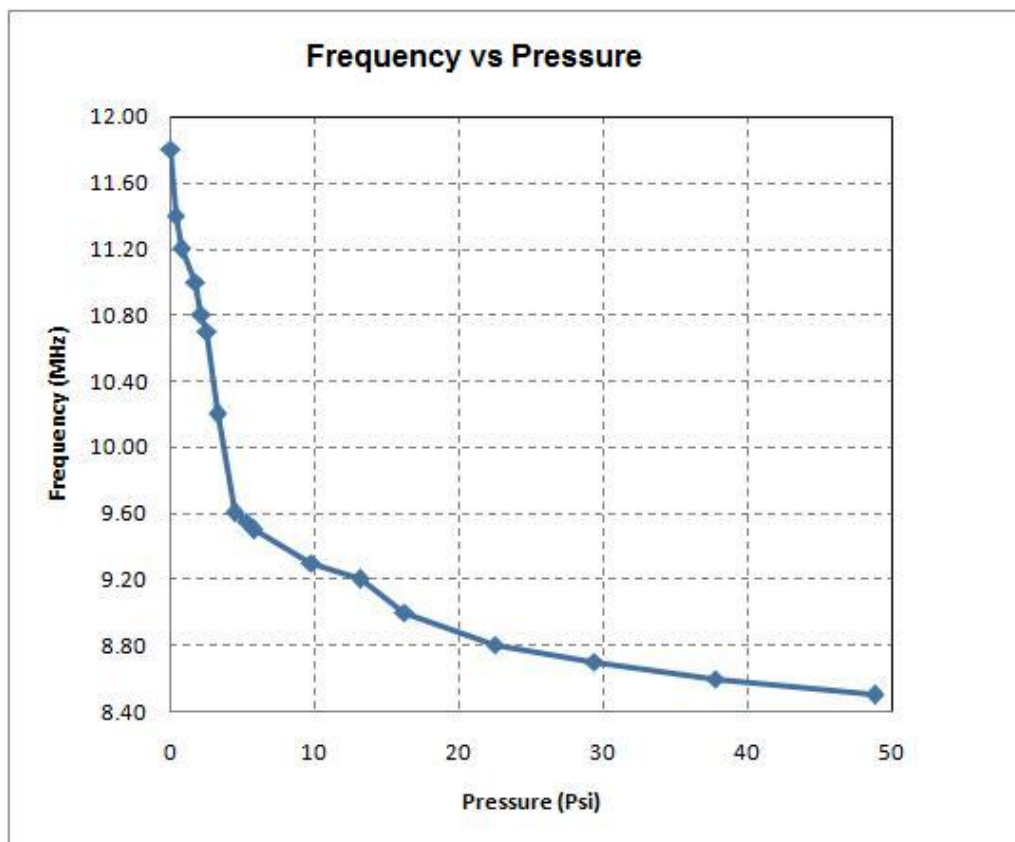


Figure 5-9: Resonant frequency of the tank vs. pressure measured with the wireless set-up for POLYURETHANE material

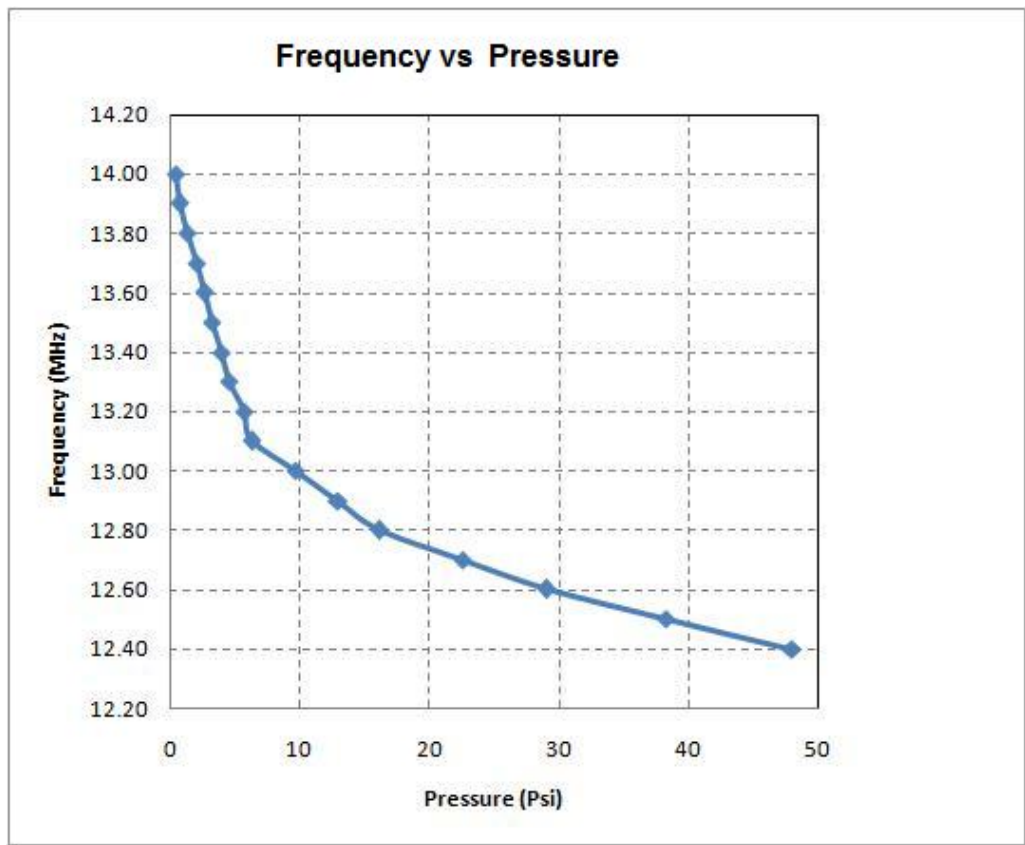


Figure 5-10: Resonant frequency of the tank vs. pressure measured with the wireless set-up for PDMS material

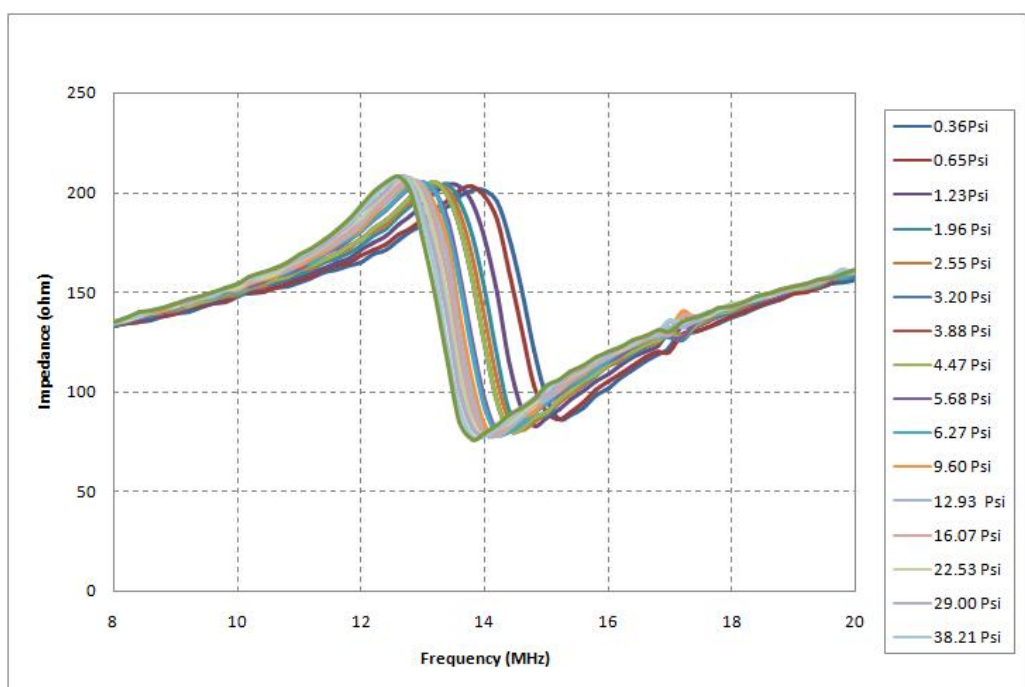


Figure 5-11: Resonant frequency of the tank vs. impedance response of the reader measured with the wireless set-up for PDMS material

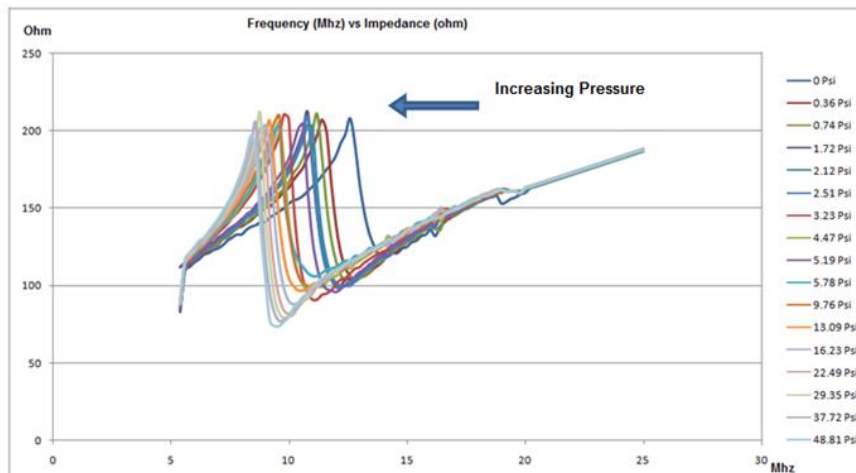


Figure 5–12: Resonant frequency of the tank vs. pressure measured with the wireless set-up for POLYURETHANE material

5.3.2 Interdigital Pressure Sensor

For the interdigital pressure sensor an experiment was performed. The figure 5-13 is shown the experimental relationship between the pressure applied and the Resonant frequency of the sensor. The sensor in our experiment is our first prototype, which is used to prove the concept and feasibility of wireless pressure sensing with desired performances.

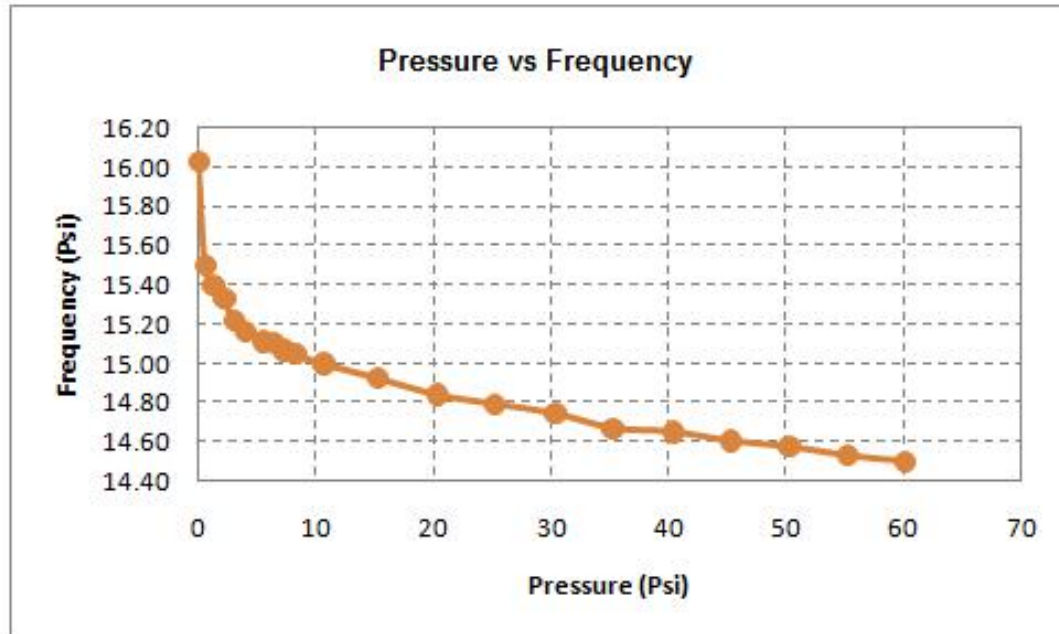


Figure 5–13: Resonant frequency vs. pressure measured for the IDC sensor

5.4 Conclusions

The experiment proved that the LC pressure sensors made of an elastomer material and IDC are feasible for wireless pressure monitoring. For the parallel plate pressure sensor the elastomer material of each capacitor is pressure dependent, that is, as the pressure increases or decreases, the dielectric material will be deformed. This causes the capacitance variations along with pressure and then the resonant frequency is a response to pressure changes.

For the IDC pressure sensor, in the experimental results it was found that the capacitance for the IDC is changed when a pressure is applied, it means that the permittivity of the sensing layer changes when pressure is applied. The results of the experiments have demonstrated the feasibility of the proposed pressure sensors and good sensitivity.

6 CONCLUSION AND FUTURE WORK

6.1 Conclusion

This project presents the development of two novel passive wireless pressure sensors which have the same structure with two major parts: a capacitor which is a pressure sensing element and an inductor which works as a passive power source and data communication element. These two components work together as an LC resonator to realize the wireless pressure sensing and remote power, eliminating the need for wire connection. The result of this research project has demonstrated feasibility of the proposed pressure sensor and good sensitivity. Battery-free and wireless pressure sensing can be realized without requiring physical connection, power supplies and active elements in the sensor circuit.

The first proposed pressure sensor has a laminated structure with an interdigital capacitor (IDC) that is a sensing element and a spiral inductor that works as a passive power source and data communication element, for this proposed sensor the sensing element is comprised of a set of linear parallel electrodes coated with pressure sensing material on the top, in this case the piezoelectric material: Polyvinylidene Fluoride (PVDF). The change of capacitance in the IDC is a function of the geometry of the electrodes and the electric properties the sensitive layer (PVDF film). The sensing element for the second proposed pressure sensor is a parallel plate which the change the capacitance is due the deformation of the dielectric material between the conductive parallel plates. For this design were used and compare two polymeric liquid materials (Polyurethane and PVDF) and they will be used and it has to be

soft enough to deform over a target pressure. The inductor coil will be formed by winding an insulated wire.

Following a review of the state-of-the-art of nowadays pressure technology, the capacitor schematic design was presented for the two proposed sensors. Modeling and simulation of the capacitance for both sensor was used in the sensor design in order to limit the resonant frequency to the reader range(5 Mhz to 50 Mhz). Moreover, sensor performance was analyzed to optimize the sensor configuration, maximize sensing distance, Q factor and sensitivity. The sensor prototype was then successfully fabricated to prove the concept of a pressure sensing device using passive wireless communication.

Research contributions achieved by this project can be summarized as follows:

- An innovative passive wireless sensor scheme has been successfully demonstrated
- Sensor performance were analyzed
- The sensor prototype was developed and calibrated

The effective design capacitors for wireless sensing applications requires a process to obtain a geometry and materials that optimize application requirements. Modeling and simulation were performed in order to minimize sensor size, maximize the detection distance, quality factor, and sensor sensitivity.

6.2 Future Work

Some research could be expanded in the future:

- Build a more accurate system for calibration
- Analyze the pressure-dependent inductance and resistance in order to calibrate the sensor much more accurately
- Research other materials with higher sensitivity

- Construction will need some optimization for improved performance and practicality of the device

APPENDICES

APPENDIX A

TITLE OF APPENDIX A

$$L = 24.1/1000; "m"; NN = 26; W = 0.0008; "m";$$

$$G = 0.0008; "m";$$

$$h = 0.00011; "m";$$

$$Eo = 8.854 * 10^{-12}; "F/m";$$

$$Es = 3.5; Epoly = 2.25 Epvdf = 10$$

$$E1 = 10; h1 = 0.00011; "m"; h2 = 0.000035; "m"; h3 = 0.0001; "m";$$

$$n = W/(W + G);$$

$$"n = 0.9"$$

$$Lamda = 2 * (W + G); r = h/Lamda;$$

$$q = Exp[-4 * Pi * r];$$

$$\begin{aligned} &\text{Interior Electrodes PDVF; } r1 = h1/Lamda \quad q1 = Exp[-4 * Pi * r1] \quad v21 = \\ &EllipticTheta[2, 0, q1]; \quad v31 = EllipticTheta[3, 0, q1]; \quad k1 = (v21/v31)^2; \quad t41 = 1/k1; \\ &Kk1 = EllipticK[k1]; \quad t21 = JacobiSN[(Kk1*n), k1]; \quad Ki1 = t21 * ((t41^2 - 1)/(t41^2 - \\ &t21^2))^{0.5}; \quad Kip1 = (1 - Ki1^2)^{0.5}; \end{aligned}$$

$$\text{Interior Electrodes Poly } Kiinf = Sin[(Pi * n)/2]; \quad Kiinf = (1 - Kiinf^2)^{0.5};$$

$$\begin{aligned} &\text{Interior Electrodes substrate; } r2 = h3/Lamda \quad q2 = Exp[-4 * Pi * r2] \quad v22 = \\ &EllipticTheta[2, 0, q2]; \quad v32 = EllipticTheta[3, 0, q2]; \quad k2 = (v22/v32)^2; \quad t42 = 1/k2; \\ &Kk2 = EllipticK[k2]; \quad t22 = JacobiSN[(Kk2*n), k2]; \quad Ki2 = t22 * ((t42^2 - 1)/(t42^2 - \\ &t22^2))^{0.5}; \quad Kip2 = (1 - Ki2^2)^{0.5}; \end{aligned}$$

$$\begin{aligned} CIidc = &Eo * L * ((2 * Epoly) * ((EllipticK[Kiinf])/(EllipticK[Kiinf])) + \\ &((Epvdf - Epoly) * ((EllipticK[Ki1])/(EllipticK[Kip1]))) + ((Es - Epoly) * ((EllipticK[Ki2])/(EllipticK[Kip2]))) \end{aligned}$$

Exterior Electrodes PDVF; $r1 = h1/Lamda$ $t4E1 = Cos[h1 * ((3.1416 * (n + 1))/8 * r1)];$ $t3E1 = Cos[h1 * ((3.1416 * (1 - n))/8 * r1)];$ $KE1 = (1/t3E1) * ((t4E1^2 - t3E1^2)/(t4E1^2 - 1))^{0.5};$ $KEp1 = (1 - KE1^2)^{0.5};$

Electrodes Poly $KEinf = (2 * n^{0.5})/(1 + n);$ $KEinfp = (1 - KEinf^2)^{0.5};$

Exterior Electrodes substrate; $r2 = h3/Lamda$ $t4E2 = Cos[h3 * ((3.1416 * (n + 1))/8 * r2)];$ $t3E2 = Cos[h3 * ((3.1416 * (1 - n))/8 * r2)];$ $KE2 = (1/t3E2) * ((t4E2^2 - t3E2^2)/(t4E2^2 - 1))^{0.5};$ $KEp2 = (1 - KE2^2)^{0.5};$

$CEidc = Eo * L * ((2 * Epoly) * ((EllipticK[KEinf])/(EllipticK[KEinfp])) + ((Epvdf - Epoly) * ((EllipticK[KE1])/(EllipticK[KEp1]))) + ((Es - Epoly) * ((EllipticK[KE2])/(EllipticK[KEp2])))$

TOTAL CAPACITANCE;

$CIDC = (((NN - 3) * (CIidc/2)) + (2 * ((CIidc * CEidc)/(CIidc + CEidc))));$ " F"

$CIDCpF = CIDC * 10^{12}$ pF"

SPIRAL INDUCTANCE $nn = 7;$ $uo = 4 * Pi] * 10^{-7};$ $R = 0.004;$ $a = 0.0006;$

$LL = nn^2 * uo * R(Log[8 * R/a] - 1.75)$

FREQUENCY;

$F = (1/(2 * Pi * (LL * CIDC)^{0.5}))/10^6$

REFERENCE LIST

- [1] Lynch; K. J. Loh. A summary review of wireless sensors and sensor networks for structural health monitoring. *Shock and Vibration Digest*, 38(2):91–128, 2006.
- [2] Celebi M. *Seismic Instrumentation of Buildings (With Emphasis on Federal Buildings)*. Technical Report No. 0-7460-68170, United States Geological Survey, Menlo Park, CA.
- [3] P. MacGillivray and K. Goddard. Advanced sensor technology for marine propulsion control systems. *in Proceedings of the 11th Ship Control Systems Symposium, Southampton, UK*, 2:245–257, 1997.
- [4] H. H.; Inman D. J.. Park, G.; Cudney. Impedance-based health monitoring of civil structural components. *Journal of Infrastructure Systems*, 6(4):153–160, 2000.
- [5] . Wu, F. ; Chang. A built-in active sensing diagnostic system for civil infrastructure systems. *in Smart Structures and Materials, San Diego, CA, March 5-7*, 4330:27–35, 2001.
- [6] M. Fernandez-Bolaos A. Ionescu J. M. Quero A. Luque, R. G. Bolea. Capacitive pressure microsensor fabricated by bulk micromachining and sacrificial layer etching. *IEEE Industrial Electronics, IECON - 32nd Annual Conference on*, pages 2969 – 2974, 2006.
- [7] Norbert; Kappert Holger; Mokwa-Wlfried Kasten, Klaus; Kordas. Capacitive pressure sensor with monolithically integrated cmos readout circuit for high temperature applications. *sensors and Actuators, A: Physical*, 97-98:83–87, 2002.

- [8] D.T. Wang E. Lund J. Nysther L. Furuberg M. Visser T. Fallet R.W. Bernstein S.T. Moe), K. Schjllberg-Henriksen. Capacitive pressure sensor with monolithically integrated cmos readout circuit for high temperature applications. *sensors and Actuators, A: Physical*, 97-98:83–87, 2002.
- [9] W.K. Schomburg A.V. Shirinov. Pressure sensor from a pvdf film. *Sensors and Actuators, A: Physical*, 142(1):48–55, 2008.
- [10] Chia-Chu Chiang; Chou-Ching K. Lin and Ming-Shuang Ju. An implantable capacitive pressure sensor for biomedical applications. *Sensors and Actuators A: physical*, 134(2):382–388, 2007.
- [11] B.; Behrend D.; Scheiter T.; Steger M.; Oppermann K.; Kapels H.; Landgraf E.; Wenzel D.; Etuodt D. Hierold, C.; Clasbrumme. Implantable low power integrated pressure sensor system for minimalinvasive telemetric patient monitoring. *The Eleventh Annual International Workshop on Micro Electro Mechanical Systems*, pages 568 – 573, 1998.
- [12] S.; Humayun M.S.; Yu-Chong Tai Po-Jui Chen; Rodger, D.C.; Saati. Implantable parylene-based wireless intraocular pressure sensor. *IEEE 21st International Conference on Micro Electro Mechanical Systems*, pages 58–61, 2008.
- [13] Mehran Mehregany Li Chen. A silicon carbide capacitive pressure sensor for in-cylinder pressure measurement. *Sensors and Actuators, A: Physical*, 145-146(1-2):2–8, 2008.
- [14] J.; Olthuis W.; Bergveld P.; van den Berg A Herber, S.; Eijkel. Study of chemically induced pressure generation of hydrogels under isochoric conditions using a microfabricated device. *J.Chem. Phys*, 121(6):2746–2751, 2004.
- [15] W.; Siegel R.A.; Ziaie B Lei, M.; Choi. An ultrasensitive microsensor based on self-aligned drypatterned environmentally sensitive hydrogels. *IEEE Int. Conf. Solid-State Sensor. Actuator. Microsyst. (Transducers)*, pages 1824–1827, 2005.

- [16] C.M.A Ashruf. Thin flexible pressure sensors. *Sensor Review*, 22(4):322–327, 2002.
- [17] load torque databook Omegadyne pressure, force. www.omegadyne.com/intsafe.html. 1996.
- [18] CT. Omega Inc., Stamford. The pressure, strain, and force handbook. 1996.
- [19] T.J.P. Gwilliam and P.G. Collar. A strain gauge pressure sensor for measuring tides on the continental shelf. *Institute of Oceanographic Sciences Report*, 14, Wormley, UK, page 27pp, 1974.
- [20] <http://www.omega.com/literature/transactions/volume3/pressure.html>.
- [21] Jan-Fong Jue. A novel potentiometric pressure sensor with a temperature-independent signal for geothermal drillin. *Materials and Systems Research, Inc.*
- [22] Qing-An Huang Min-Xin Zhou. A novel capacitive pressure sensor based on sandwich structures. *Journal Of Microelectromechanical Systems*, 14(6), 2005.
- [23] E. Lysko, J.M. Stolarski and R.S. Jachowicz. Capacitive silicon pressure sensor based on the one-side waferprocessing. *Solid-State Sensors and Actuators, 1991. Digest of Technical Papers, TRANSDUCERS '91., 1991 International Conference on*, pages 685–688, 1991.
- [24] K.; Schlichting V.; Obermeier E.; Barton K. Hein, S.; Holzner. Capacitive differential pressure sensor with high overloadcapability using silicon/glass technology. *Solid State Sensors and Actuators, 1997. TRANSDUCERS '97 Chicago., 1997 International Conference on*, 2:1477–1480, 1997.
- [25] D. Neukomm P.A. Chatzandroulis, S. Tsoukalas. A miniature pressure system with a capacitive sensor and a passive telemetry link for use in implantable applications. *Journal of Microelectromechanical Systems*, 9(1):18–23, 2000.
- [26] S. T. Moe, K. Schjlbjerg-Henriksen, D. T. Wang, E. Lund, J. Nysther, L. Furu-berg, M. Visser, T. Fallet, and R. W. Bernstein. Capacitive differential pressure

- sensor for harsh environments. *Sensors and Actuators A: Physical*, 83(1-3):30 – 33, 2000.
- [27] K Finkenzeller. Fundamentals and applications in contactless smart cards and identification. *In RFID Handbook, 2nd Ed.*, Ed.; John Wiley Sons Ltd: Chichester, England:70, 2002.
- [28] Grizzle K. M. Wood S. L. Novak, L. J. and D. P. Neikirk. Development of state sensors for civil engineering structures. *Smart Systems and Non-destructive Evaluation for Civil Infrastructures, San Diego, CA, March 36, Proceedings of the SPIE*, 5057:358363, 2003.
- [29] B. Carkhuff and Cain. Corrosion sensors for concrete bridges. *IEEE Instrumentation and Measurement Magazine*, 6(2):1924, 2003.
- [30] M. Saafi and Romine. Embedded mems for health monitoring and management of civil infrastructure. *Smart Structures and Materials: Sensors and Smart Structures Technologies for Civil, Mechanical, and Aerospace Systems, Proceedings of the SPIE*, 5391:331343, 2004.
- [31] M. Kothamasu R. Paily S. R. Munnangi, G. Haobijam and R. S. Kshetri-mayum. Cmos capacitive pressure sensor design and integration with rfid tag for biomedical applications.
- [32] RoyWant. Rfid explained a primer on radio frequency identification technologies. *Edi. Morgan Claypool*, 2006.
- [33] C. Ruppel F. Seifert, W.E. Bulst. Embedded mems for health monitoring and management of civil infrastructure. *Sensors and Actuators A*,, 44:231–239, 1994.
- [34] T. Ostertag et al G. Scholl, F. Schmidt. Wireless passive saw sensor systems for industrial and domestic applications. *EEE Proc. Frequ. Control Symp.*, pages 595–601, 1998.

- [35] R. Weigel G. Schimetta, F. Dollinger. A wireless pressure measurement system using a saw hybrid sensor.
- [36] Alfred Pohl. A review of wireless saw sensors.
- [37] Orhan Akar, Tayfun Akin, and Khalil Najafi. A wireless batch sealed absolute capacitive pressure sensor. *Sensors and Actuators A: Physical*, 95(1):29 – 38, 2001.
- [38] M. von Arx M. A. Fonseca, J. M. English and M. G. Allen. Wireless micromachined ceramic pressure sensor for high-temperature applications. *Journal of Microelectromechanical Systems*, 11(4), August 2002.
- [39] B. Y. Nabipoor, M.; Majlis. A new passive telemetry lc pressure and temperature sensor optimized for tpms. *Journal of Physics: Conference Series*, 34(1):770–775, 2006.
- [40] Y.B. Takahata, K.; Gianchandani. A micromachined capacitive pressure sensor using a cavity-less structure with bulk-metal/elastomer layers and its wireless telemetry application. *Sensors*, 8(4):2317–2330, 2008.
- [41] Technology Enabled Active Learning MIT. Mit physics 8.02t electricity magnetism: Course notes, May 2006. <http://web.mit.edu/8.02t/www/802TEAL3D/>.
- [42] P H Veltink J C Löttersy, W Olthuis and P Bergveld. Implantable parylene-based wireless intraocular pressure sensor. *Mechanical properties of the rubber elastic polymer polydimethylsiloxane for sensor applications*, 7(3):145–147, 1997.
- [43] J.; Bullen D.; Liu C Engel, J.M.; Chen. Polyurethane rubber as a mems material: Characterization and demonstration of an all-polymer two-axis artificial hair cell flow sensor. *IEEE Int. Conf. Micro Elec. Mech. Syst. (MEMS)*, pages 279–282, 2005.

- [44] S.; Su J.; Zhang. Q.M Cheng, Z.Y.; Gross. Pressure-temperature study of dielectric relaxation of a polyurethane elastomer. *Polymer Sci. B Polymer Phys.*, 37(10):983–990, 1999.
- [45] C. Liu D. Armani. Re-configurable fluid circuits by pdms elastomer micromachining. *12th Int. Conference on MEMS*, pages 222–227, 1999.
- [46] F.W. Grover. In inductance calculations: Working formulas and tables. *Dover Publications Inc.: New York*, 1946.
- [47] S. Chatzandroulisa M. Chatzichristidia I. Raptisa Th. Ganetsosb R. Igrejac M. Kitsaraa, D. Goustouridisa and C.J. Diasc. Single chip interdigitated electrode capacitive chemical sensor arrays. *Sensors and Actuators B: Chemical*, 127(1):186–192, 2007.
- [48] W.; Olthuis W.; Bergveld P.; van den Berg Timmer, B.H.; Sparreboom. Planar interdigitated conductivity sensors for low electrolyte concentrations. *Proceedings of SeSens*, pages 878–883, 2001.
- [49] K Sundara-Rajan. Estimation of moisture content in paper pulp containing calcium carbonate using fringing field impedance spectroscopy. *Appita Journal*, pages 413–419, 2004.
- [50] L.; Mamishev A.V Sundara-Rajan, K.; Byrd II. Moisture content estimation in paper pulp using fringing field impedance spectroscopy. *IEEE Sensors Journal*, pages 378–383, 2003.
- [51] K.; Yamada S.; Iwahara M. Taniguchi, T.; Nakamura. An image synthesis method for eddy current testing based on extraction of defect orientation. *Digest of IEEE Intermag conference*, 2002.
- [52] Ke Sun. Design and characterization of passive wireless strain sensor. Master’s thesis, University Of Puerto Rico Mayagüez Campus, 2007.

- [53] Rui Igreja and C. J. Dias. Analytical evaluation of the interdigital electrodes capacitance for a multi-layered structure. *Sensors and Actuators A*, 112:291–301, 2004.
- [54] Ya Wang. A passive wireless temperature sensor for harsh environment applications, 2007.
- [55] Surya Musunuri. Design issues for monolithic dc/dc converters. *IEEE Transactions on Power Electronics*, 20(3):639–649, 2005.
- [56] J.; Bullen D.; Liu C Engel, J.M.; Chen. Polyurethane rubber all-polymer artificial hair cell sensor.